SCAP promotes CARTS biogenesis at endoplasmic reticulum-Golgi contact sites

Yuichi Wakana[1]*, Kaito Hayashi[1], Takumi Nemoto[1], Chiaki Watanabe[1], Masato Taoka[2], Felix Campelo[3], Hidetoshi Kumata[1], Tomonari Umemura[1], Hiroki Inoue[1], Kohei Arasaki[1], and Mitsuo Tagaya[1]*

[1]School of Life Sciences, Tokyo University of Pharmacy and Life Sciences, Hachioji, Tokyo 192-0392, Japan.

[2]Faculty of Science, Department of Chemistry, Tokyo Metropolitan University, Hachioji, Tokyo 192-0397, Japan.

[3]ICFO-Institut de Ciencies Fotoniques, The Barcelona Institute of Science and Technology, Barcelona, Spain

*Corresponding authors:

Yuichi Wakana and Mitsuo Tagaya

E-mail: ywakana@toyaku.ac.jp

Phone: +81 426 76 7116

Fax: +81 426 76 8866

K. Hayashi and T. Nemoto contributed equally to this paper

The number of words: 3,713

Abstract

In response to cholesterol deprivation, SCAP escorts SREBP transcription factors from the endoplasmic reticulum (ER) to the Golgi complex for their proteolytic activation, leading to gene expression for cholesterol synthesis and uptake. Here we show that in cholesterol-fed cells ER-localized SCAP interacts through Sac1 phosphoinositide 4-phosphate (PI4P) phosphatase with a VAP/OSBP complex, which mediates counter-transport of ER cholesterol and Golgi PI4P at ER-Golgi contact sites. SCAP knockdown inhibited the turnover of PI4P perhaps due to a cholesterol transport defect and altered the subcellular distribution of the VAP/OSBP complex. As in the case of perturbation of lipid transfer complexes at ER-Golgi contact sites, SCAP knockdown inhibited the biogenesis of the *trans*-Golgi network-derived transport carriers CARTS, which was reversed by expression of wild-type SCAP but not cholesterol sensing-defective mutants. Altogether, our findings reveal an unexpected new role of SCAP under cholesterol-fed conditions in the facilitation of CARTS biogenesis at ER-Golgi contact sites.

Introduction

Cholesterol plays a crucial role in regulating the functions of mammalian cell membranes by determining their integrity and fluidity. Cholesterol together with sphingolipids can form liquid-ordered membrane nanodomains which are segregated from other lipids and thus are proposed to serve as platforms for specific proteins that regulate signal transduction and endocytosis at the plasma membrane (PM), and apical transport from the *trans*-Golgi network (TGN)[1–8]. Increasing evidence –including recent experiments where sphingomyelin (SM) metabolism at the *trans*-Golgi membranes was perturbed– strongly suggests that such lipid nanodomains are required for the functional organization of enzymatic domains, cargo sorting, and transport carrier biogenesis at the TGN[9–14], and thereby are crucial to maintain homeostatic control of the function of the Golgi complex.

Although the endoplasmic reticulum (ER) receives cholesterol from the PM and other sources, and produces it *de novo*, the ER cholesterol content remains low[15]. This is accomplished through the export of cholesterol from the ER against the concentration gradient in both vesicular and non-vesicular manners, the latter of which occurs at membrane contact sites. In particular, at ER-Golgi contact sites, Golgi-associated oxysterol-binding protein (OSBP) interacts with an integral ER membrane protein named vesicle-associated membrane protein–associated protein (VAP), and transfers cholesterol from the ER to the *trans*-Golgi membranes, accompanied by reciprocal transfer of phosphoinositide 4-phosphate (PI4P)[16]. PI4P transported to the ER is hydrolyzed by the ER-localized lipid phosphatase Sac1, which thus seems to provide a driving force for cholesterol transport[17]. ER-Golgi contact sites also function in ceramide transport from the ER to the *trans*-Golgi membranes mediated by a complex of VAP and ceramide transfer protein (CERT), which leads to the biosynthesis of SM and diacylglycerol (DAG) by SM synthase at the *trans*-Golgi membranes[18–20]. Of note, DAG recruits a serine/threonine kinase, protein kinase D (PKD), which phosphorylates CERT and OSBP to release these proteins from the Golgi complex[21,22]. PKD also contributes to the membrane fission reaction required for transport carrier biogenesis at the TGN[23–25]. We previously reported that lipid transfer at ER-Golgi contact sites is

required for the biogenesis of carriers of the TGN to the cell surface (CARTS)[26], which transport selective cargoes from the TGN to the PM[27,28]. Lipid transfer at these contact sites needs to be strictly controlled on demand for TGN-to-PM transport, but the molecular mechanisms underlying this regulation remain largely elusive.

In this study, we identified sterol regulatory element binding protein (SREBP) cleavage-activating protein (SCAP) as a novel Sac1-interacting protein. SCAP is a polytopic membrane protein that functions as a cholesterol sensor in the ER to control the cholesterol content in mammalian cells[29–34]. When the ER cholesterol level is low, SCAP escorts the membrane-bound transcription factors SREBPs into COPII vesicles for their export from the ER to the Golgi complex, where SREBPs are cleaved by proteases, allowing their transcriptionally active domain to enter the nucleus and promote expression of genes involved in cholesterol synthesis and uptake. Conversely, when cholesterol in the ER membrane is abundant, cholesterol binds to SCAP and triggers conformational changes that allow SCAP to interact with the integral ER membrane protein Insig, which retains SCAP in the ER along with unprocessed SREBPs. Our data show an unexpected new function of SCAP under cholesterol-fed conditions, in which SCAP interacts via Sac1 with the VAP/OSBP complex and facilitates the biogenesis of CARTS at ER-Golgi contact sites.

Results

Identification of SCAP as a novel component of Sac1-positive ER-Golgi contact sites. We previously reported that Sac1 is a major component of specialized ER subdomains that are closely apposed to the TGN, most likely corresponding to ER-Golgi contact sites[26]. Therefore, the perinuclear Sac1 localization likely represents its presence at ER-Golgi contact sites, rather than at the Golgi complex as previously reported[35]. To identify novel components of ER-Golgi contact sites, we explored Sac1-interacting proteins using an Sac1 K2A mutant with replacement of two lysines in the C-terminal COPI-interacting motif with alanines. While the di-lysine COPI-interacting motif is used for retrograde transport from the *cis*-Golgi to the ER[36], some ER integral membrane proteins also utilize this signal for their movement along the ER from the cell center to the periphery[37,38]. Green fluorescent protein (GFP)-fused Sac1 K2A was highly enriched in the juxtanuclear region, compared with the wild-type protein (WT), as revealed by its reduced peripheral staining (Fig. 1a). The deconvolved, enhanced contrast, and increased resolution images of cells treated with 25-hydroxycholesterol (25-HC), a reagent that stabilizes ER-Golgi contact sites by promoting the targeting of the VAP/OSBP complex to these sites through binding to OSBP[16,39,40], showed good overlapping of the GFP-Sac1 K2A signal with that of the integral ER membrane protein VAP-A, and close apposition of GFP-Sac1 K2A to the TGN marker TGN46, as shown for WT (Fig. 1b). Consistently, the membrane continuity of GFP-Sac1 K2A-positive juxtanuclear compartments with the peripheral ER was demonstrated by inverse fluorescence recovery after photobleaching (iFRAP) (Fig. 1c): photobleaching of the peripheral area immediately decreased the perinuclear signals of GFP-Sac1 WT and K2A, but not of the Golgi marker N-acetylglucosaminyl transferase I-GFP (negative control).

Immunoprecipitation of FLAG-tagged Sac1 K2A followed by mass spectrometric analysis revealed multiple interactors of FLAG-Sac1 K2A (Fig. 1d, lane 2) with decreased binding of COPI coat proteins, which are major interactors for FLAG-Sac1 WT (Fig. 1d, lane 1, asterisks). The identified Sac1 K2A-interacting proteins include known components of ER-Golgi contact sites such as VAP-A, VAP-B, and OSBP,

together with proteins of unknown functions at the contact sites, including SCAP (Fig. 1e). We focused on SCAP because it had been previously shown to interact with VAP-A and VAP-B, although the physiological role of this interaction remains unexplored[41].

ER-localized SCAP interacts through Sac1 with the VAP-A/OSBP complex at ER-Golgi contact sites. In order to confirm that SCAP is a bona fide component of ER-Golgi contact sites, the interactions of FLAG-SCAP with VAP-A, OSBP, and Sac1 were examined by immunoprecipitation (Fig. 2a). Endogenous Sac1 and VAP-A were clearly coprecipitated with FLAG-SCAP, but not with the FLAG vector control (Fig. 2a, lanes 7 and 9). When Myc-OSBP was coexpressed, this protein was coprecipitated with FLAG-SCAP and the interaction of FLAG-SCAP with VAP-A, but not with Sac1, was enhanced (Fig. 2a, lanes 9 and 10). As negative controls, we showed that an integral ER membrane protein, reticulon-4B (RTN-4B), and another lipid transfer protein, CERT, were not coprecipitated with FLAG-SCAP (Fig. 2b).

Next, we asked whether SCAP interacts with the VAP-A/OSBP complex via Sac1. Our previous work showed that Sac1 interacts with VAP-A via OSBP[26]. We used two OSBP mutants, FF/AA and PH-FFAT, that are defective in binding to VAP and Sac1, respectively (Ref[42,43] and Supplementary Fig. 1a,b). In cells expressing Myc-OSBP FF/AA, this protein, but not VAP-A, was found to interact with FLAG-SCAP (Fig 2a, lane 11), suggesting that VAP-A is not needed for the interaction of SCAP with OSBP. By contrast, Myc-OSBP PH-FFAT was not coprecipitated with FLAG-SCAP (Fig 2a, lane 12). Although previous work revealed that Myc-OSBP PH-FFAT fixes and expands ER-Golgi contact sites through its stable interaction with VAP-A[16], it inhibited the interaction of FLAG-Sac1 with VAP-A (Supplementary Fig. 1, lane 12). Myc-OSBP PH-FFAT defective in Sac1 binding also greatly reduced the interaction of FLAG-SCAP with VAP-A (Fig. 2a, lane 12), emphasizing the requirement of Sac1 for the interaction of SCAP with the VAP-A/OSBP complex. Similar results were obtained for a FLAG-tagged C-terminal cytoplasmic fragment (C-term) of SCAP[44] (Fig. 2c), excluding possible membrane aggregation and cosedimentation with FLAG-SCAP.

To corroborate that ER-localized SCAP, but not Golgi-localized SCAP, can form complexes with VAP-A, OSBP, and Sac1 at ER-Golgi contact sites, we used a SCAP mutant with replacement of aspartic acid 451 and leucine 452 with alanines at the MELADL motif in loop 6 (D451A/L452A), which is defective in COPII binding and therefore cannot exit the ER in COPII-coated vesicles[45]. FLAG-SCAP D451A/L452A showed interactions with VAP-A, OSBP, and Sac1, analogous to FLAG-SCAP WT (Fig. 2d). We next visualized the interactions of SCAP with these proteins in intact cells by using bimolecular fluorescence complementation (BiFC). As shown previously[46,47], a BiFC signal derived from the Vn-OSBP/Vc-VAP-A interaction was detected at the perinuclear region representing ER-Golgi contact sites (Supplementary Fig. 2c, top row), whereas no signal was detected when only Vn- or Vc-fused constructs were individually expressed (Supplementary Fig. 2a,b). This signal was enhanced by 25-HC treatment (Supplementary Fig. 2c, middle row). Similar results were obtained with the combination of Vn-OSBP/Vc-Sac1 (Supplementary Fig. 2d). The Vn-SCAP/Vc-Sac1 and Vn-SCAP/Vc-VAP-A interactions were also observed at ER-Golgi contact sites upon coexpression of Myc-OSBP, and these interactions were enhanced by 25-HC treatment (Fig. 2e,f), similar to the Vn-OSBP/Vc-VAP-A and Vn-OSBP/Vc-Sac1 interactions (Supplementary Fig. 2c,d).

To further substantiate that the perinuclear Vn-SCAP/Vc-Sac1 and Vn-SCAP/Vc-VAP-A BiFC signals represent the interaction of ER-localized SCAP, but not Golgi-localized SCAP, we examined the effect of cholesterol depletion. As reported previously[48], cholesterol depletion using lipoprotein-deficient serum and 2-hydroxypropyl-β-cyclodextrin caused redistribution of a part of the SCAP pool from the ER to the *cis/medial* Golgi membranes (Supplementary Fig. 3a,b) accompanied by SREBP2 cleavage (Supplementary Fig. 3c). In contrast to 25-HC treatment, cholesterol depletion did not enhance either the Vn-SCAP/Vc-Sac1 or Vn-SCAP/Vc-VAP-A interaction (Fig. 2e,f, bottom row). Altogether, these results suggest that ER-localized SCAP preferentially interacts with VAP-A, OSBP, and Sac1 at ER-Golgi contact sites.

SCAP is important for PI4P turnover and VAP-A/OSBP complex distribution at ER-Golgi contact sites. The finding that SCAP forms complexes with VAP-A, OSBP, and Sac1 at ER-Golgi contact sites prompted us to examine whether SCAP is involved in the counter transport of ER cholesterol and Golgi PI4P at ER-Golgi contact sites. To address this issue, we performed knockdown of SCAP in HeLa cells. By using siRNA, the expression of SCAP was decreased to ~20% of the control level (Fig. 3a). In response to cholesterol deprivation, the SCAP-SREBP pathway stimulates transcription of genes responsible for cholesterol synthesis and uptake, such as 3-hydroxy-3-methylglutaryl coenzyme A reductase (HMGR) and low-density lipoprotein receptor (LDLR)[30,49]. However, under cholesterol-fed conditions [that is, culturing of cells in normal medium supplemented with fetal calf serum (FCS) as a source of sterols], SCAP knockdown did not reduce the transcription of either HMGR or LDLR genes, but rather slightly increase the LDLR mRNA levels (Fig. 3b). Consistently, no significant change in the total cholesterol level was observed upon SCAP knockdown (Fig. 3c). Similar results were obtained for a stable cell line (shSCAP cells) with reduced SCAP expression (~10% of that in parental HeLa cells) (Fig. 3d,e).

Because there are no good probes with sufficient sensitivity to detect low levels of cholesterol in ER and Golgi membranes, we monitored the PI4P level in SCAP knockdown cells. When PI4P was visualized with a specific antibody, the fluorescence signal in shSCAP cells was significantly increased compared with in the parental cells, especially in the juxtanuclear region that partially overlapped with membranes positive for the TGN marker sialyltransferase (Fig. 3f,g). Similar phenotypes were observed upon VAP-A/B or CERT/OSBP double knockdown, as well as in Sac1 knockdown cells (Supplementary Fig. 4), suggesting that SCAP knockdown inhibited the turnover of PI4P at ER-Golgi contact sites.

Next, we evaluated the effect of SCAP knockdown on the formation of the VAP-A/OSBP complex by using the BiFC approach. A stable cell line coexpressing Vn-OSBP and Vc-VAP-A showed BiFC signals in the juxtanuclear region, which was enhanced by 25-HC treatment (Supplementary Fig. 5). When SCAP was knocked down by siRNA, ~34% of cells showed bright BiFC signals in the peripheral region, besides

the juxtanuclear Golgi region, and the number of cells with this phenotype increased to ~62% upon 25-HC treatment (Fig. 3h). As the VAP/OSBP complex has been reported to exist not only at ER-Golgi contact sites, but also at ER-endosome contact sites[50], we compared the localization of the BiFC signals with that of the late endosomal marker CD63. The results showed the close apposition of CD63 but not of TGN46 to the peripheral BiFC signals (Fig. 3i), suggesting that SCAP is required to prevent the redistribution of the VAP-A/OSBP complex to ER-endosome contact sites and to maintain it at ER-Golgi contact sites.

SCAP is required for the biogenesis of CARTS at the TGN. We previously reported that a defect in lipid transfer at ER-Golgi contact sites inhibits the biogenesis of CARTS at the TGN[26]. We visualized CARTS in Vn-OSBP/Vc-VAP-A expressing cells treated with 25-HC by staining a CARTS specific cargo, pancreatic adenocarcinoma up-regulated factor (PAUF)[27]. Images subjected to deconvolution processing showed that putative nascent CARTS were located in the close vicinity of BiFC signals (Fig. 4a), suggesting that CARTS form at sites immediately adjacent to the VAP-A/OSBP-containing ER-Golgi contact sites. Next, we investigated whether SCAP is required for CARTS-mediated protein secretion. In SCAP knockdown cells, the secretion of PAUF-MycHis was reduced to ~50% of that in control cells (Fig. 4b). PAUF-MycHis secreted by SCAP knockdown cells was detected as a smeared band, suggesting a defect in PAUF processing, as previously observed in cells depleted of other ER-Golgi contact site components[26].

The effect of SCAP knockdown on the biogenesis of CARTS was assessed with an inducible CARTS formation assay, where synchronized transport of PAUF from the ER is carried out by using a reverse dimerization system involving D/D solubilizer-induced disassembly of FM4 domains[51]. The chimera protein mKate2-FM4-PAUF initially retained in the ER was first exported from this organelle and accumulated in the Golgi membranes on D/D solubilizer treatment at 20°C for 45 min, after which the temperature was shifted to 37°C to induce the formation of mKate2-FM4-PAUF-containing CARTS at the TGN. Live cell imaging showed that a large number of

CARTS were formed at the TGN membranes and dispersed throughout the cytoplasm (Supplementary Video 1). Next, mKate2-FM4-PAUF was expressed in control and SCAP knockdown cells. At 15 min after the temperature shift to 37°C, the average number of CARTS in SCAP knockdown cells was ~20% of that in control cells (Fig. 4c).

Lipid transfer at ER-Golgi contact sites is thought to regulate CARTS biogenesis through organization of cholesterol- and SM-enriched nanodomains at the TGN[26]. We therefore examined the effect of SCAP knockdown on transport of glycosylphosphatidyl inositol (GPI)-anchored protein, which is most likely associated with such lipid nanodomains[1,52,11]. Synchronized transport of mKate2-FM4-GPI from the ER to the PM was initiated by addition of the D/D solubilizer, as previously reported[11]. SCAP knockdown did not affect transport of mKate2-FM4-GPI from the ER (0 min) to the Golgi complex (30 min). Nevertheless, at 60 min after transport initiation, the amount of mKate2-FM4-GPI that had reached the cell surface was significantly decreased in SCAP knockdown cells (Fig. 4d). At 90 min most of the protein had been transported to the PM in control cells, but in ~40% of SCAP knockdown cells, the protein was still localized to the TGN (Fig. 4d,e). Similar results were obtained with knockdown of VAP-A/B, CERT/OSBP, or, to a lesser extent, OSBP (Fig. 4d and Supplementary Fig. 6a). In addition to these results, overexpression of OSBP PH-FFAT, which immobilizes ER-Golgi contact sites and inhibits CARTS biogenesis[26], strongly inhibited mKate2-FM4-GPI export from the TGN (Supplementary Fig. 6b). When mKate2-FM4-GPI and PAUF-MycHis were coexpressed in cells, mKate2-FM4-GPI was included in PAUF-MycHis-positive CARTS, although its fluorescence signal was relatively low (Supplementary Fig. 7a). Consistent with our previous finding that CARTS biogenesis requires PKD-mediated membrane fission at the TGN[27], TGN-derived tubules induced by a dominant-negative kinase-dead mutant of PKD2 also contained mKate2-FM4-GPI (Supplementary Fig. 7b). Taken together, these results suggest that SCAP promotes the biogenesis of CARTS which contain cholesterol- and SM-enriched nanodomains.

SCAP regulates CARTS biogenesis in a cholesterol-dependent manner. SCAP directly binds cholesterol and plays a pivotal role in cholesterol homeostasis as a cholesterol sensor in the ER membrane[34,53,54]. Does SCAP regulate CARTS biogenesis by sensing the ER cholesterol level? Previous mutagenesis analysis of SCAP in Chinese hamster ovary (CHO) cells revealed that several amino acid residues are critical for a conformational change induced by cholesterol binding[34]. Specifically, replacement of tyrosine 234 in the cholesterol-binding loop1 region of SCAP (Fig. 5a) with alanine (Y234A) abolishes binding of loop1 to loop7, and thus this mutant binds to Insig even in the absence of cholesterol[54]. By contrast, a mutant with replacement of tyrosine 298 in the transmembrane sterol-sensing domain (Fig. 5a) with cysteine (Y298C) is resistant to the cholesterol-induced conformational change and shows no Insig binding even in the presence of sterols[41,55–58]. We established different shSCAP cells, each of which stably expressing hamster SCAP WT, Y234A, or Y298C. Western blotting of cell lysates with an antibody specific to hamster SCAP, and one recognizing both human and hamster SCAP indicated that Y234A was less expressed than WT and Y298C, but it was still expressed at a considerably higher level than the endogenous protein in parental HeLa cells (Fig. 5b). Immunofluorescent staining with an anti-hamster SCAP antibody showed reticular distributions of WT, Y234A, and Y298C in the ER, under cholesterol-fed conditions (Supplementary Fig. 8, upper row). In previous work, digestion of *N*-linked carbohydrates of SCAP by endoglycosidase (endo) H indicated that SCAP Y298C is redistributed to the Golgi complex even in the presence of sterols[55]. However, at the level of immunofluorescence microscopy, the signal of Y298C in the Golgi complex was not obvious, because most of the protein was present in the juxtanuclear ER (Supplementary Fig. 8, upper right panel). Perhaps, a minor fraction of the Y298C pool is transported to the Golgi complex and acquires endo H resistance in the presence of sterols. When cholesterol was depleted from cells, fractions of the WT and Y298C pools were redistributed from the ER to the Golgi complex, but Y234A remained in the ER (Supplementary Fig. 8, lower row), consistent with previous reports[54,55,57].

By using these cell lines, we first examined the effect that the expression of the respective hamster SCAP proteins has on the turnover of PI4P. Our results showed that expression of WT, but not Y234A or Y298C, reversed the accumulation of PI4P at the TGN (Fig. 5c). We next examined their effects on CARTS biogenesis. Expression of SCAP WT caused the recovery of the number of CARTS from SCAP knockdown, but neither Y234A nor Y298C showed such an effect (Fig. 5d). These results suggest that the sterol-sensing ability of SCAP is required for CARTS biogenesis.

Discussion

SCAP was discovered in 1996 as an ER protein whose mutation conferred, on CHO cells, resistance to 25-HC, an oxygenated cholesterol derivative that suppresses SREBP processing and thereby blocks cholesterol synthesis, but cannot replace cholesterol for cell viability[29]. Later studies demonstrated that SCAP senses the ER cholesterol content and, in response to cholesterol deficiency, escorts SREBPs from the ER to the Golgi complex for their cleavage-mediated activation[30–34].

In the present study, we demonstrated a new function of SCAP under cholesterol-fed conditions. Our data suggests a model whereby SCAP at ER-Golgi contact sites interacts with VAP/OSBP via Sac1, and regulates counter-transport of cholesterol and PI4P in an ER cholesterol-dependent manner. This idea is supported by the finding that SCAP knockdown causes the accumulation of PI4P at the TGN (Fig. 3f), a hallmark of the impairment of cholesterol/PI4P exchange between the ER and the *trans*-Golgi membranes. SCAP appears to contribute to the establishment of rigid ER-Golgi contact sites because its knockdown caused partial redistribution of the VAP/OSBP complex to ER-endosome contact sites (Fig. 3i). At the *trans*-Golgi membranes, cholesterol and SM organize lipid nanodomains, which function as a platform for molecular machineries responsible for processing and sorting of cargoes including GPI-anchored proteins (Fig. 6, right panel). In parallel, DAG, which is synthesized together with SM from ceramide and phosphatidylcholine, recruits PKD for membrane fission, leading to CARTS biogenesis. Intriguingly, our finding of putative nascent CARTS in the close vicinity to ER-Golgi contact sites (Fig. 4a) suggests the possible role of the ER contact in determining the position for membrane fission, analogous to its important role in mitochondrial and endosomal fission[59,60].

Cytoplasmic coats generally provide a means to coordinate signal-mediated cargo sorting with carrier budding and membrane fission. However, most TGN-derived transport carriers, including CARTS, lack cytoplasmic coats and therefore such molecular mechanisms remain largely elusive for these transport carriers[27,61]. A recent paper reported that Ca^{2+}-dependent and oligomerization-driven cargo sorting, which is mediated by the SPCA1 Ca^{2+} pump and the secreted Ca^{2+} binding protein Cab45, is

coupled to local SM synthesis at the TGN[14]. The finding that sorting of lysozyme C, one of the secretory cargoes in CARTS[27], is under control through this mechanism strongly supports our model.

Our data showed that neither the SCAP Y234A nor Y298C mutant, which reflect different conformations in the context of Insig binding, are competent for PI4P turnover and CARTS biogenesis (Fig. 5c,d). These findings imply that conformational switching that reflects cholesterol-free and -bound states is important. Considering that the ER contains a low level of cholesterol, it is tempting to speculate that SCAP functions in collecting cholesterol in the ER membrane to give it to cytosolic OSBP for efficient cholesterol transfer at ER-Golgi contact sites. It is of note that SCAP knockdown dramatically altered the distribution of the VAP/OSBP complex in the presence of 25-HC (Fig. 3h). As 25-HC directly binds to OSBP[39,40], but indirectly to SCAP via Insig[62,63], this finding reveals the possibility that SCAP functions at ER-Golgi contact sites as a complex with Insig (and probably also SREBPs). A previous finding that Insig interacts with VAP-A and VAP-B[64] might suggest the presence of such a complex.

In conclusion, our findings reveal a new role of SCAP under cholesterol-fed conditions and provide insights into the regulatory mechanisms for lipid transfer at ER-Golgi contact sites for transport carrier biogenesis at the TGN.

Online Methods

Antibodies and reagents

Monoclonal antibodies were procured as follows: FLAG and alpha-tubulin were purchased from Sigma-Aldrich; Myc and hamster SCAP (clone: 9D5) from Santa Cruz Biotechnology; His from QIAGEN; and PI4P from Echelon Biosciences. Polyclonal antibodies were procured as follows: HA, Nogo (RTN-4B), SCAP, and GST from Santa Cruz Biotechnology; TGN46 (sheep IgG) from AbD Serotec; GFP from Molecular Probes; SREBP2 from Abcam; and Myc from Cell Signaling Technology. To raise rabbit polyclonal antibodies against TGN46 and Sac1, GST-tagged fragments of human TGN46 (aa 1-365) and Sac1 (aa 1-55), respectively, were expressed in *Escherichia coli*, purified, and used as antigens. These antibodies were isolated by affinity chromatography on antigen-coupled beads. An anti-VAP-A polyclonal antibody was produced as described previously[26]. An anti-Mannosidase II polyclonal antibody was provided by V. Malhotra (Centre for Genomic Regulation, Barcelona, Spain). D/D solubilizer, 25-HC, and 2-hydroxypropyl-β-cyclodextrin were purchased from Clontech, Sigma-Aldrich, and Wako Chemicals, respectively.

Plasmids

The plasmids encoding PAUF-MycHis, N-acetylglucosaminyl transferase I-GFP, Myc-OSBP[65], HA-CERT[66], and mKate2-FM4-GPI were kindly donated by S. S. Koh (Korea Research Institute of Bioscience and Biotechnology, Daejeon, Korea), N. Nakamura (Kyoto Sangyo University, Kyoto, Japan), H. Arai (University of Tokyo, Tokyo, Japan), K. Hanada (National Institute of Infectious Diseases, Tokyo, Japan), and Cristopher G. Burd (Yale School of Medicine, New Haven, CT, USA), respectively. The plasmids encoding the GFP-Sac1 WT and K2A mutant were generous gifts from P. Mayinger (Oregon Health and Science University, OR, USA). The plasmid encoding GST-PKD2 kinase dead was provided by V. Malhotra (Centre for Genomic Regulation, Barcelona, Spain). The cDNAs encoding hamster SCAP WT and C-term (aa 732-1276) were amplified by PCR from pCMV-GFP-SCAP, a generous gift from Peter Espenshade (Johns Hopkins University School of Medicine, MD, USA), and inserted into pFLAG-

CMV-6c to express the protein with an N-terminal FLAG. For expression of FLAG-SCAP D451A/L452A, point mutations were introduced into pFLAG-SCAP by PCR using primers designed for replacing aspartic acid 451 and leucine 452 with alanines. The cDNA encoding hamster SCAP or rabbit OSBP (WT or FF/AA) were inserted into pCI-IRES-Bsr in combination with one encoding the N-terminal fragment of Venus (Vn) (aa 1-172). The cDNA encoding human Sac1 or VAP-A was inserted into pCI-IRES-Bsr in combination with one encoding the C-terminal fragment of Venus (Vc) (aa 154-238). For establishment of stable cell lines, the cDNAs encoding Vn-OSBP and Vc-VAP-A were inserted into the pMXs-IRES-Puro and pCX4-IRES-Bsr retroviral vectors, respectively, and hamster SCAP with or without N-terminal GFP was inserted into pCX4-IRES-Bsr. For expression of SCAP Y234A or Y298C, each point mutation was introduced into pCX4-SCAP-IRES-Bsr by PCR using primers designed for replacing tyrosine 234 or 298 with alanine. For expression of mKate2-FM4-PAUF, the cDNA encoding GPI in the plasmid for mKate2-FM4-GPI was replaced with one encoding human PAUF (aa 43-197). The cDNA encoding human sialyltransferase (aa 1-69) was inserted into a pcDNA3-based plasmid encoding mRFP to express the protein with a C-terminal mRFP. Plasmids for Myc-OSBP FF/AA and PH-FFAT were described previously[26]. For establishment of shSCAP HeLa cells, the Mission shRNA plasmid (TRCN0000289279) was purchased from Sigma-Aldrich.

siRNA and shRNA

The targeting sequences of siRNA and shRNA were as follows:

Control (GL2 luciferase): 5'-AACGTACGCGGAATACTTCGA-3'

SCAP (siRNA): 5'-AACCTCCTGGCAGTAGATGTA-3'

SCAP (shRNA): 5'- GCTCTGGTGTTCTTGGACAAA-3'

VAP-A: 5'-AACTAATGGAAGAGTGTAAAA-3'

VAP-B: 5'-AAGAAGGTTATGGAAGAATGT-3'

OSBP: 5'-AATACTGGGAGTGTAAAGAAA-3'

CERT: 5'-AAGAACAGAGGAAGCATATAA-3'

Sac1: 5'-AACTGATATTCAGTTACAAGA-3'

Cell culture and transfection

HeLa and HEK 293T cells were grown in DMEM supplemented with 10% FCS. PLAT-A packaging cells were grown in DMEM supplemented with 10% FCS, 10 μg/ml blasticidin S, and 1 μg/ml puromycin. Plasmid and siRNA transfection into HeLa cells were carried out using X-tremeGENE 9 DNA transfection reagent (Roche) and Oligofectamine reagent (Invitrogen), respectively, according to the manufacturers' protocols. Plasmid transfection into HEK 293T cells was carried out using polyethylenimine (Polysciences) or Lipofectamine 2000 transfection reagent (Invitrogen), according to the manufacturers' protocols.

Establishment of stable cell lines

For establishment of HeLa cells stably expressing GFP-SCAP, PLAT-A packaging cells were transfected with pCX4-GFP-SCAP-IRES-Bsr, and 48 h later, the medium containing retrovirus was collected and used for infection of HeLa cells. Selection of HeLa cells stably expressing GFP-SCAP was performed with 10 μg/ml blasticidin S. A HeLa stable cell line coexpressing Vn-OSBP and Vc-VAP-A was established in a similar manner with pMXs-Vn-OSBP-IRES-Puro and pCX4-Vc-VAP-A-IRES-Bsr by selecting cells with 1 μg/ml puromycin and 10 μg/ml blasticidin S. For establishment of shSCAP HeLa cells, HEK 293T cells were cotransfected with the Mission shRNA plasmid (TRCN0000289279), pMDLg/pRRE, pRSV-Rev, and pCMV-VSVG. After 48 h, the medium containing lentivirus was collected and used for infection of HeLa cells. Selection of shSCAP HeLa cells was performed with 1 μg/ml puromycin. Establishment of shSCAP HeLa cells stably expressing hamster SCAP WT, Y234A, or Y298C was performed as described for GFP-SCAP HeLa cells with pCX4-SCAP (WT, Y234A, or Y298C)-IRES-Bsr. All the stable cell lines were obtained without single-cell cloning.

Immunofluorescence microscopy

HeLa cells were fixed with 4% paraformaldehyde (PFA) in phosphate-buffered saline (PBS) at room temperature for 20 min, permeabilized with 0.2% Triton X-100 in PBS for 30 min, and then blocked with 2% bovine serum albumin (BSA) in PBS for 30 min. The cells were labeled with the indicated primary antibodies and secondary antibodies conjugated to Alexa Fluor 488, 594, or 633. The samples were analyzed with an Olympus Fluoview FV1000 or FV1200 confocal microscope with a UPLSAPO 60x O NA 1.35 objective and FV10-ASW software. Image processing and measurement of fluorescence intensity were performed with ImageJ software (National Institutes of Health).

Image deconvolution

Deconvolution processing was performed with Huygens Professional version 18.04 (Scientific Volume Imaging, The Netherlands, http://svi.nl). For that, a theoretical point-spread function (PSF) was automatically computed based on the microscope and image acquisition parameters. The deconvolution process was numerically performed using the Classic Maximum Likelihood Estimation (CMLE) algorithm. In brief, this algorithm assumes that the photon noise is Poisson-distributed, and the likelihood of an estimate of the actual image given the computed PSF and the acquired image is iteratively optimized until either a quality factor or a maximum number of iterations is reached. In our deconvolutions, we used a quality factor equal to 0.001 and a maximum 50 iterations. The signal-to-noise ratio (SNR) for each acquired image was computed based on three line profiles going through regions of background signals towards regions of positive, actual signals. Typically, SNR were of the order of 7–20 for the different analyzed images.

PI4P staining

PI4P staining was performed as described previously[13,67]. In brief, HeLa cells were fixed with 2% PFA at room temperature for 15 min, followed by washing with PBS containing 50 mM NH_4Cl. The cells were then permeabilized with 20 μM digitonin in buffer A (20 mM PIPES, pH 6.8, 137 mM NaCl, 2.7 mM KCl). After removal of

digitonin by washing with buffer A, the cells were blocked with 5% FCS in buffer A for 45 min. The cells were labeled with an anti-PI4P antibody and a secondary antibody conjugated to Alexa Fluor 488. After post-fixation with 2% PFA for 5 min, the cells were washed with PBS containing 50 mM NH_4Cl and with water, and then mounted on a microscope slide. The samples were analyzed by fluorescence microscopy as described above.

iFRAP

HeLa cells expressing GFP-Sac1 WT, K2A, or N-acetylglucosaminyl transferase I-GFP in Opti-MEM were cultured in 5% CO_2 at 37°C during live-cell imaging. The cells were subjected to bleaching with high laser intensity (473 nm laser) for 15 s, followed by an imaging scan with a time interval between frames of 10 s for ~4 min by use of an Olympus Fluoview FV1000 confocal microscope with a UPLSAPO 100x O NA 1.40 objective and FV10-ASW software. Image processing and measurement of fluorescence intensity were performed with ImageJ software.

Immunoprecipitation

HEK 293T cells were lysed in buffer B (50 mM HEPES-KOH, pH 7.4, 100 mM NaCl, 1.5 mM $MgCl_2$, 1 mM dithiothreitol, 1% Nonidet P-40, 1 μg/ml leupeptin, 2 μM pepstatin A, 2 μg/ml aprotinin, and 1 mM phenylmethylsulfonyl fluoride). The lysates were centrifuged at 17,000 × g for 10 min. The resulting supernatants were immunoprecipitated with an anti-FLAG M2 affinity gel (Sigma-Aldrich), and the precipitated proteins were analyzed by Western blotting with the indicated primary antibodies and secondary antibodies conjugated to horseradish peroxidase. For identification of the Sac1 interacting proteins, the precipitated proteins were eluted with FLAG peptide and analyzed by silver staining. Protein bands were excised from the gel and subjected to LC-MS/MS analysis.

LC-MS/MS analysis

Each gel piece was incubated with 0.25 µg trypsin in 20 µl Tris-HCl (pH 8.8) overnight at 37°C[68], and the resulting peptide mixture was analyzed with a direct nanoflow LC-MS/MS system equipped with an hybrid quadrupole-orbitrap mass spectrometer (Q Exactive, Thermo Scientific, Boston, MA) as previously described[69]. Briefly, peptides were separated on a reversed-phase tip column (150 µm i.d. × 70 mm, Mightysil-C18, 3-µm particle) using a 0–35% linear gradient of acetonitrile in 0.1% (v/v) formic acid for 35 or 70 min at a flow rate of 100 nL/min. Full MS scans were acquired with a resolution of 30,000 at a mass-to-charge ratio of 400. The ten most intense ions were fragmented in the data-dependent mode by collision-induced dissociation with normalized collision energy of 35, activation q of 0.25, and activation time of 10 ms and one microscan. The MS/MS data were converted to the mascot generic format with the Proteome Discoverer software (Thermo Scientific, ver. 1.1). The files were processed with the MASCOT algorithm (version 2.2.1., Matrix Science Ltd., London, United Kingdom) to assign peptides using the Swiss-Prot sequence database (release 2012.11, human) under the search parameters described in Ref[69]. Peptides were identified based on the MASCOT definitions. For the search parameters, we set the variable modifications for acetylation (protein N terminus) and oxidation (Met). The maximum missed cleavage was set at 1 with a peptide mass tolerance of +/- 15 ppm. Peptide charges from +2 to +4 states and MS/MS tolerances of +/- 0.8 Da were allowed. All results of peptide searches were extracted from the Mascot DAT files using the STEM software[70].

Cholesterol depletion

Lipoprotein-deficient serum (LPDS) was prepared as described previously[71,72]. In brief, FCS was adjusted to a density of 1.25 g/mL with solid KBr and then centrifuged for 16 h at 10°C at 50,000 rpm in a Beckman VTi 50 rotor. The upper yellow-orange layer containing lipoproteins and the salt pellet were removed, and the remaining fraction was dialyzed extensively at 4°C against 150 mM NaCl for 48 h. HeLa cells were incubated with DMEM containing 5% LPDS and 1% 2-hydroxypropyl-β-cyclodextrin for 3 h.

Quantitative real-time PCR

RNA was prepared using an RNeasy Mini kit (QIAGEN) and cDNA was synthesized with SuperScript III reverse transcriptase (Invitrogen) primed by oligo(dT)15. Quantitative real-time PCR was performed with a Rotor-Gene Q RT-PCR machine (QIAGEN) using a KAPA SYBR FAST qPCR kit (Kapa Biosystems), according to the manufacturer's protocol. The primers used were as follows: SCAP, forward primer 5'-TATCTCGGGCCTTCTACAACC-3' and reverse primer 5'-GGGGCGAGTAATCCTTCACA-3'; HMGR, forward primer 5'-TGACCTTTCCAGAGCAAGC-3' and reverse primer 5'-CCAACTCCAATCACAAGACATTC-3'; LDLR, forward primer 5'-GTGTCACAGCGGCGAATG-3' and reverse primer 5'-CGCACTCTTTGATGGGTTCA-3'; HPRT1, forward primer 5'-TTCCAGACAAGTTTGTTGTAGGAT-3' and reverse primer 5'-GCAGATGGCCACAGAACTAG-3'. Values were normalized as the HPRT1 expression level.

Total cholesterol measurement

HeLa cells were lysed in water for 30 min at 37°C and then subjected to total cholesterol measurement with an Amplex Red cholesterol assay kit (Molecular probes), according to the manufacturer's protocol. Values were normalized to protein content determined as using a Pierce BCA protein assay kit (Thermo Fisher Scientific).

PAUF secretion assay

HeLa cells were transfected with control siRNA or siRNA oligos targeting SCAP. At 48 h after siRNA transfection, the cells were transfected with a plasmid for PAUF-MycHis, 20 h later the medium was replaced with Opti-MEM, and then the cells were incubated at 37°C for 6 h. After collecting the medium, the cells were lysed with 0.5% sodium dodecyl sulfate (SDS) and 0.025 units/μL benzonase nuclease (Sigma-Aldrich) in PBS. The medium and cell lysates were analyzed by Western blotting with an anti-

His antibody.

GPI transport assay

HeLa cells were transfected with control siRNA or siRNA oligos targeting SCAP, VAP-A/VAP-B, OSBP or CERT/OSBP. At 48 h after siRNA transfection, the cells were transfected with a plasmid for mKate2-FM4-GPI, 20 h later the medium was replaced with DMEM containing 10% FCS, 1 μM D/D solubilizer, and 20 μg/mL cycloheximide, and then cells were incubated at 37°C for the indicated times. The cells were then fixed with 4% PFA and analyzed by fluorescence microscopy as described above.

Inducible CARTS formation assay

HeLa cells were transfected with control siRNA or siRNA oligos targeting SCAP. At 48 h after siRNA transfection, the cells were transfected with a plasmid for mKate2-FM4-PAUF, 20 h later the medium was replaced with DMEM containing 10% FCS, 20 mM HEPES-KOH, pH 7.4, 1 μM D/D solubilizer, and 20 μg/mL cycloheximide, and then the cells were incubated in a water bath at 20°C for 45 min. The cells were then incubated in a water bath at 37°C for the indicated times, followed by fixation with 4% PFA. The samples were analyzed by fluorescence microscopy as described above. Quantification of CARTS was performed with ImageJ software (National Institutes of Health). The fluorescence signal of mKate2-FM4-PAUF-containing punctae was distinguished from the background by setting a threshold and analyzed at a set size within 0.05-2.00 μm^2. For live-cell imaging, HeLa cells were transfected with a plasmid for mKate2-FM4-PAUF, 20 h later the medium was replaced with Opti-MEM containing 1 μM D/D solubilizer and 20 μg/mL cycloheximide, and then the cells were incubated in a water bath at 20°C for 45 min. The cells were then incubated at 37°C and 5% CO_2 to monitor CARTS biogenesis. Images were acquired continuously with a time interval between frames of 30 sec for ~75 min by use of an Olympus Fluoview FV1200 confocal microscope with a UPLSAPO 60x O NA 1.35 objective and FV10-ASW software. The images were processed with ImageJ software.

Acknowledgements

We thank Peter Mayinger, Hiroyuki Arai, Kentaro Hanada, Nobuhiro Nakamura, Sang Seok Koh, and Vivek Malhotra for providing materials. We appreciate the technical assistance of Nanako Oyama, So Yoshida, Yuika Komatsuda, Yuiko Kawai, Natsumi Hoshino, Tomoya Iizuka, Sho Furuichi, and Katsunori Iwasa. We are grateful to Josse van Galen and Vivek Malhotra for comments on the manuscript. This work was supported in part by Grants-in-Aid for Scientific Research [grant numbers 15K18507 and 17K07348 to Y.W., and 18H02439 to M.T.] from the Ministry of Education, Culture, Sports, Science, and Technology of Japan, the Naito Foundation [to Y.W.], and the Ono Medical Research Foundation [to Y.W.]. F.C. acknowledges financial support from the Spanish Ministry of Economy and Competitiveness ("Severo Ochoa" program for Centres of Excellence in R&D (SEV-2015-0522), FIS2015-63550-R, FIS2017-89560-R, and BFU2015-73288-JIN, AEI/FEDER/UE), Fundació Privada Cellex, and from the Generalitat de Catalunya through the CERCA program.

Author contributions

Y.W. and M.Tagaya conceived and designed the experiments. Y.W., K.H., T.N., C.W., F.C., and H.K. performed the experiments. M.Taoka performed LC-MS/MS analysis and analyzed the data. T.U., H.I., K.A., and M.Tagaya provided samples. Y.W., F.C., and M.Tagaya wrote the manuscript.

Competing interests

The authors declare no competing interests.

References

1. Simons, K. & Ikonen, E. Functional rafts in cell membranes. **387**, 4 (1997).

2. Keller, P. & Simons, K. Cholesterol Is Required for Surface Transport of Influenza Virus Hemagglutinin. *J. Cell Biol.* **140**, 1357–1367 (1998).

3. Wang, Y., Thiele1, C. & Huttner, W. B. Cholesterol is Required for the Formation of Regulated and Constitutive Secretory Vesicles from the trans-Golgi Network. *Traffic* **1**, 952–962 (2000).

4. Ikonen, E. Roles of lipid rafts in membrane transport. *Curr. Opin. Cell Biol.* **13**, 470–477 (2001).

5. Klemm, R. W. *et al.* Segregation of sphingolipids and sterols during formation of secretory vesicles at the trans-Golgi network. *J. Cell Biol.* **185**, 601–612 (2009).

6. Lingwood, D. & Simons, K. Lipid Rafts As a Membrane-Organizing Principle. *Science* **327**, 46–50 (2010).

7. Simons, K. & Sampaio, J. L. Membrane organization and lipid rafts. *Cold Spring Harb. Perspect. Biol.* **3**, a004697 (2011).

8. Jacobson, K., Liu, P. & Lagerholm, B. C. The Lateral Organization and Mobility of Plasma Membrane Components. *Cell* **177**, 806–819 (2019).

9. Duran, J. M. *et al.* Sphingomyelin organization is required for vesicle biogenesis at the Golgi complex: Lipid organization controls vesicle biogenesis. *EMBO J.* **31**, 4535–4546 (2012).

10. van Galen, J. *et al.* Sphingomyelin homeostasis is required to form functional enzymatic domains at the trans-Golgi network. *J. Cell Biol.* **206**, 609–618 (2014).

11. Deng, Y., Rivera-Molina, F. E., Toomre, D. K. & Burd, C. G. Sphingomyelin is sorted at the *trans* Golgi network into a distinct class of secretory vesicle. *Proc. Natl. Acad. Sci.* **113**, 6677–6682 (2016).

12. Campelo, F. *et al.* Sphingomyelin metabolism controls the shape and function of the Golgi cisternae. *eLife* **6**, (2017).

13. Capasso, S. *et al.* Sphingolipid metabolic flow controls phosphoinositide turnover at the *trans* -Golgi network. *EMBO J.* **36**, 1736–1754 (2017).

14. Deng, Y. *et al.* Activity of the SPCA1 Calcium Pump Couples Sphingomyelin Synthesis to Sorting of Secretory Proteins in the Trans-Golgi Network. *Dev. Cell* **47**, 464-478.e8 (2018).

15. Ikonen, E. Mechanisms of cellular cholesterol compartmentalization: recent insights. *Curr. Opin. Cell Biol.* **53**, 77–83 (2018).

16. Mesmin, B. *et al.* A Four-Step Cycle Driven by PI(4)P Hydrolysis Directs Sterol/PI(4)P Exchange by the ER-Golgi Tether OSBP. *Cell* **155**, 830–843 (2013).

17. Antonny, B., Bigay, J. & Mesmin, B. The Oxysterol-Binding Protein Cycle: Burning Off PI(4)P to Transport Cholesterol. *Annu. Rev. Biochem.* **87**, 809–837 (2018).

18. Hanada, K. *et al.* Molecular machinery for non-vesicular trafficking of ceramide. *Nature* **426**, 803–809 (2003).

19. Kawano, M., Kumagai, K., Nishijima, M. & Hanada, K. Efficient Trafficking of Ceramide from the Endoplasmic Reticulum to the Golgi Apparatus Requires a VAMP-associated Protein-interacting FFAT Motif of CERT. *J. Biol. Chem.* **281**, 30279–30288 (2006).

20. Hanada, K., Kumagai, K., Tomishige, N. & Yamaji, T. CERT-mediated trafficking of ceramide. *Biochim. Biophys. Acta BBA - Mol. Cell Biol. Lipids* **1791**, 684–691 (2009).

21. Fugmann, T. *et al.* Regulation of secretory transport by protein kinase D–mediated phosphorylation of the ceramide transfer protein. *J. Cell Biol.* **178**, 15–22 (2007).

22. Nhek, S. *et al.* Regulation of Oxysterol-binding Protein Golgi Localization through Protein Kinase D–mediated Phosphorylation. *Mol. Biol. Cell* **21**, 2327–2337 (2010).

23. Baron, C. L. & Malhotra, V. Role of Diacylglycerol in PKD Recruitment to the TGN and Protein Transport to the Plasma Membrane. *Science* **295**, 325–328 (2002).

24. Malhotra, V. & Campelo, F. PKD Regulates Membrane Fission to Generate TGN to Cell Surface Transport Carriers. *Cold Spring Harb. Perspect. Biol.* **3**, a005280–a005280 (2011).

25. Pagliuso, A. *et al.* Golgi membrane fission requires the CtBP1-S/BARS-induced activation of lysophosphatidic acid acyltransferase δ. *Nat. Commun.* **7**, 12148 (2016).

26. Wakana, Y. *et al.* CARTS biogenesis requires VAP–lipid transfer protein complexes functioning at the endoplasmic reticulum–Golgi interface. *Mol. Biol. Cell* **26**, 4686–4699 (2015).

27. Wakana, Y. *et al.* A new class of carriers that transport selective cargo from the trans Golgi network to the cell surface. *EMBO J.* **31**, 3976–3990 (2012).

28. Wakana, Y. *et al.* Kinesin-5/Eg5 is important for transport of CARTS from the trans-Golgi network to the cell surface. *J. Cell Biol.* **202**, 241–250 (2013).

29. Hua, X., Nohturfft, A., Goldstein, J. L. & Brown, M. S. Sterol Resistance in CHO Cells Traced to Point Mutation in SREBP Cleavage–Activating Protein. *Cell* **87**, 415–426 (1996).

30. Brown, M. S. & Goldstein, J. L. The SREBP Pathway: Regulation of Cholesterol Metabolism by Proteolysis of a Membrane-Bound Transcription Factor. *Cell* **89**, 331–340 (1997).

31. Goldstein, J. L., DeBose-Boyd, R. A. & Brown, M. S. Protein Sensors for Membrane Sterols. *Cell* **124**, 35–46 (2006).

32. Radhakrishnan, A., Goldstein, J. L., McDonald, J. G. & Brown, M. S. Switch-like Control of SREBP-2 Transport Triggered by Small Changes in ER Cholesterol: A Delicate Balance. *Cell Metab.* **8**, 512–521 (2008).

33. Brown, M. S. & Goldstein, J. L. Cholesterol feedback: from Schoenheimer's bottle to Scap's MELADL. *J. Lipid Res.* **50**, S15–S27 (2009).

34. Brown, M. S., Radhakrishnan, A. & Goldstein, J. L. Retrospective on Cholesterol Homeostasis: The Central Role of Scap. *Annu. Rev. Biochem.* **87**, 783–807 (2018).

35. Blagoveshchenskaya, A. *et al.* Integration of Golgi trafficking and growth factor signaling by the lipid phosphatase SAC1. *J. Cell Biol.* **180**, 803–812 (2008).

36. Gomez-Navarro, N. & Miller, E. Protein sorting at the ER–Golgi interface. *J. Cell Biol.* **215**, 769–778 (2016).

37. Wakana, Y. *et al.* Bap31 Is an Itinerant Protein That Moves between the Peripheral Endoplasmic Reticulum (ER) and a Juxtanuclear Compartment Related to ER-associated Degradation. *Mol. Biol. Cell* **19**, 1825–1836 (2008).

38. Lavieu, G. *et al.* Induction of cortical endoplasmic reticulum by dimerization of a coatomer-binding peptide anchored to endoplasmic reticulum membranes. *Proc. Natl. Acad. Sci.* **107**, 6876–6881 (2010).

39. Ridgway, N. D., Dawson, P. A., Ho, Y. K., Brown, M. S. & Goldstein, J. L. Translocation of oxysterol binding protein to Golgi apparatus triggered by ligand binding. *J. Cell Biol.* **116**, 307–319 (1992).

40. Suchanek, M. *et al.* The mammalian oxysterol-binding protein-related proteins (ORPs) bind 25-hydroxycholesterol in an evolutionarily conserved pocket. *Biochem. J.* **405**, 473–480 (2007).

41. Yang, T. *et al.* Crucial Step in Cholesterol Homeostasis: Sterols Promote Binding of SCAP to INSIG-1, a Membrane Protein that Facilitates Retention of SREBPs in ER. *Cell* **110**, 489–500 (2002).

42. Wyles, J. P., McMaster, C. R. & Ridgway, N. D. Vesicle-associated Membrane Protein-associated Protein-A (VAP-A) Interacts with the Oxysterol-binding Protein to Modify Export from the Endoplasmic Reticulum. *J. Biol. Chem.* **277**, 29908–29918 (2002).

43. Loewen, C. J. R. A conserved ER targeting motif in three families of lipid binding proteins and in Opi1p binds VAP. *EMBO J.* **22**, 2025–2035 (2003).

44. Nohturfft, A., Brown, M. S. & Goldstein, J. L. Topology of SREBP Cleavage-activating Protein, a Polytopic Membrane Protein with a Sterol-sensing Domain. *J. Biol. Chem.* **273**, 17243–17250 (1998).

45. Sun, L.-P., Li, L., Goldstein, J. L. & Brown, M. S. Insig Required for Sterol-mediated Inhibition of Scap/SREBP Binding to COPII Proteins in Vitro. *J. Biol. Chem.* **280**, 26483–26490 (2005).

46. Kentala, H., Pfisterer, S. G., Olkkonen, V. M. & Weber-Boyvat, M. Sterol liganding of OSBP-related proteins (ORPs) regulates the subcellular distribution of

ORP–VAPA complexes and their impacts on organelle structure. *Steroids* **99**, 248–258 (2015).

47. Weber-Boyvat, M., Kentala, H., Peränen, J. & Olkkonen, V. M. Ligand-dependent localization and function of ORP–VAP complexes at membrane contact sites. *Cell. Mol. Life Sci.* **72**, 1967–1987 (2015).

48. Nohturfft, A., Yabe, D., Goldstein, J. L., Brown, M. S. & Espenshade, P. J. Regulated Step in Cholesterol Feedback Localized to Budding of SCAP from ER Membranes. *Cell* **102**, 315–323 (2000).

49. Horton, J. D. *et al.* Combined analysis of oligonucleotide microarray data from transgenic and knockout mice identifies direct SREBP target genes. *Proc. Natl. Acad. Sci.* **100**, 12027–12032 (2003).

50. Dong, R. *et al.* Endosome-ER Contacts Control Actin Nucleation and Retromer Function through VAP-Dependent Regulation of PI4P. *Cell* **166**, 408–423 (2016).

51. Rivera, V. M. *et al.* Regulation of Protein Secretion Through Controlled Aggregation in the Endoplasmic Reticulum. *Science* **287**, 826–830 (2000).

52. Mayor, S. & Riezman, H. Sorting GPI-anchored proteins. *Nat. Rev. Mol. Cell Biol.* **5**, 110 (2004).

53. Radhakrishnan, A., Sun, L.-P., Kwon, H. J., Brown, M. S. & Goldstein, J. L. Direct Binding of Cholesterol to the Purified Membrane Region of SCAP: Mechanism for a Sterol-Sensing Domain. *Mol. Cell* **15**, 259–268 (2004).

54. Motamed, M. *et al.* Identification of luminal loop 1 of scap as the sterol sensor that maintains cholesterol homeostasis. *J. Biol. Chem.* jbc.M111.238311 (2011). doi:10.1074/jbc.M111.238311

55. Nohturfft, A., Brown, M. S. & Goldstein, J. L. Sterols regulate processing of carbohydrate chains of wild-type SREBP cleavage-activating protein (SCAP), but not sterol-resistant mutants Y298C or D443N. *Proc. Natl. Acad. Sci.* **95**, 12848–12853 (1998).

56. Brown, A. J., Sun, L., Feramisco, J. D., Brown, M. S. & Goldstein, J. L. Cholesterol Addition to ER Membranes Alters Conformation of SCAP, the SREBP Escort Protein that Regulates Cholesterol Metabolism. *Mol. Cell* **10**, 237–245 (2002).

57. Yabe, D., Brown, M. S. & Goldstein, J. L. Insig-2, a second endoplasmic reticulum protein that binds SCAP and blocks export of sterol regulatory element-binding proteins. *Proc. Natl. Acad. Sci.* **99**, 12753–12758 (2002).

58. Adams, C. M., Goldstein, J. L. & Brown, M. S. Cholesterol-induced conformational change in SCAP enhanced by Insig proteins and mimicked by cationic amphiphiles. *Proc. Natl. Acad. Sci.* **100**, 10647–10652 (2003).

59. Friedman, J. R. *et al.* ER Tubules Mark Sites of Mitochondrial Division. *Science* **334**, 358–362 (2011).

60. Rowland, A. A., Chitwood, P. J., Phillips, M. J. & Voeltz, G. K. ER Contact Sites Define the Position and Timing of Endosome Fission. *Cell* **159**, 1027–1041 (2014).

61. Pakdel, M. & von Blume, J. Exploring new routes for secretory protein export from the trans-Golgi network. *Mol. Biol. Cell* **29**, 235–240 (2018).

62. Adams, C. M. *et al.* Cholesterol and 25-Hydroxycholesterol Inhibit Activation of SREBPs by Different Mechanisms, Both Involving SCAP and Insigs. *J. Biol. Chem.* **279**, 52772–52780 (2004).

63. Radhakrishnan, A., Ikeda, Y., Kwon, H. J., Brown, M. S. & Goldstein, J. L. Sterol-regulated transport of SREBPs from endoplasmic reticulum to Golgi: Oxysterols block transport by binding to Insig. *Proc. Natl. Acad. Sci.* **104**, 6511–6518 (2007).

64. Gong, Y., Lee, J. N., Brown, M. S., Goldstein, J. L. & Ye, J. Juxtamembranous aspartic acid in Insig-1 and Insig-2 is required for cholesterol homeostasis. *Proc. Natl. Acad. Sci.* **103**, 6154–6159 (2006).

65. Nishimura, T. *et al.* Oxysterol-binding protein (OSBP) is required for the perinuclear localization of intra-Golgi v-SNAREs. *Mol. Biol. Cell* **24**, 3534–3544 (2013).

66. Kumagai, K., Kawano, M., Shinkai-Ouchi, F., Nishijima, M. & Hanada, K. Interorganelle Trafficking of Ceramide Is Regulated by Phosphorylation-dependent Cooperativity between the PH and START Domains of CERT. *J. Biol. Chem.* **282**, 17758–17766 (2007).

67. Hammond, G. R. V., Schiavo, G. & Irvine, R. F. Immunocytochemical techniques reveal multiple, distinct cellular pools of PtdIns4 *P* and PtdIns(4,5) P_2. *Biochem. J.* **422**, 23–35 (2009).

68. Taoka, M., Wakamiya, A., Nakayama, H. & Isobe, T. Protein profiling of rat cerebella during development. *ELECTROPHORESIS* **21**, 1872–1879 (2000).

69. Taoka, M. *et al.* Global PROTOMAP profiling to search for biomarkers of early-recurrent hepatocellular carcinoma. *J. Proteome Res.* **13**, 4847–4858 (2014).

70. Shinkawa, T. *et al.* STEM: A Software Tool for Large-Scale Proteomic Data Analyses. *J. Proteome Res.* **4**, 1826–1831 (2005).

71. Goldstein, J. L., Basu, S. K. & Brown, M. S. [19] Receptor-mediated endocytosis of low-density lipoprotein in cultured cells. *Methods in Enzymology* **98**, 241–260 (Elsevier, 1983).

72. Poumay, Y. & Ronveaux-Dupal, M. F. Rapid preparative isolation of concentrated low density lipoproteins and of lipoprotein-deficient serum using vertical rotor gradient ultracentrifugation. *J. Lipid Res.* **26**, 1476–1480 (1985).

Figure legends

Fig. 1 | Identification of SCAP as a novel component of Sac1-positive ER-Golgi contact sites. a, Juxtanuclear localization of the GFP-Sac1 WT and K2A mutant in HeLa cells. **b**, Colocalization of GFP-Sac1 WT or K2A with VAP-A and their proximity localization with TGN46. HeLa cells expressing GFP-Sac1 WT or K2A were treated with 2 μg/mL 25-HC for 2.5 h. Images were subjected to deconvolution processing as described in *Online Methods*. The graphs on the right show the fluorescence intensity of GFP-Sac1 WT or K2A (green), and VAP-A or TGN46 (magenta) along the white line in the respective merged images. N, nucleus. **c**, iFRAP in HeLa cells expressing the GFP-Sac1 WT, K2A mutant, or N-acetylglucosaminyl transferase I (NA)-GFP. The areas delimited by a red line were bleached as described in *Online Methods*. The graph below shows quantification of the fluorescence intensity of the indicated proteins in the non-bleached, juxtanuclear region. Data are means ± s.e.m. (n = 4 cells per condition). **d**, Silver staining of immunoprecipitated proteins with the FLAG-Sac1 WT, K2A or FLAG vector in HEK 293T cells. Asterisks denote protein bands containing COPI components. SCAP was identified in the protein band boxed with a red line. **e**, Peptides of VAP-A, VAP-B, OSBP, and SCAP, which were identified by mass spectrometric analysis of FLAG-Sac1 K2A immunoprecipitates (lane 2 in panel **d**). Scale bars, 10 μm.

Fig. 2 | ER-localized SCAP interacts through Sac1 with the VAP-A/OSBP complex at ER-Golgi contact sites. a, Interactions of FLAG-SCAP with Myc-OSBP, Sac1, and VAP-A in HEK 293T cells. Cell lysates were subjected to immunoprecipitation with an anti-FLAG M2 affinity gel, and the cell lysates (Input) and immunoprecipitates (IP) were immunoblotted (IB) with the indicated antibodies. The interaction with VAP-A was enhanced by coexpression of FLAG-SCAP with Myc-OSBP WT, but not with the FF/AA or PH-FFAT mutant. Asterisks denote degraded Myc-OSBP fragments. **b**, Interactions of FLAG-SCAP with Myc-OSBP, Sac1, and VAP-A, but not with HA-CERT or RTN-4B. **c**, Interactions of FLAG-SCAP C-term with Myc-OSBP, Sac1, and VAP-A. **d**, Interactions of the FLAG-SCAP D451A/L452A mutant with Myc-OSBP,

Sac1, and VAP-A. **e**,**f**, BiFC visualization of SCAP/Sac1 (**e**) or SCAP/VAP-A (**f**) interactions at ER-Golgi contact sites in HeLa cells coexpressing Myc-OSBP and Venus N-terminal fragment (Vn)-fused SCAP in combination with Venus C-terminal fragment (Vc)-fused Sac1 (**e**) or VAP-A (**f**). The cells were treated without (top panels) or with (middle panels) 2 μg/mL 25-HC for 2.5 h, or were cholesterol depleted (Chol Depl) for 3 h (bottom panels). The expression of Vn-SCAP together with Vc-Sac1 (**e**) or Vc-VAP-A (**f**) was visualized with an anti-GFP antibody. Scale bars, 10 μm.

Fig. 3 | SCAP is important for PI4P turnover and VAP-A/OSBP complex distribution at ER-Golgi contact sites. a, siRNA-mediated knockdown of SCAP in HeLa cells, monitored by Western blotting. The graph shows determination of the expression levels of SCAP at 72 h after siRNA transfection. Data are means ± s.e.m. (n = 3 independent experiments, ***$P < 0.001$, two-tailed Student's *t*-test). Asterisks on the Western blot denote nonspecific bands. **b**, Determination of the mRNA levels of the indicated genes in control (Cont) and SCAP knockdown cells by quantitative real-time PCR. Data are means ± s.e.m. (n = 4 independent experiments, **$P < 0.01$, ***$P < 0.005$, two-tailed Student's *t*-test, NS, not significant). **c**, Total cholesterol (Chol) levels in control and SCAP knockdown cells. Data are means ± s.e.m. (n = 6 independent experiments, NS, not significant, two-tailed Student's *t*-test). **d**, Establishment of shSCAP HeLa cells. The graph shows determination of the expression levels of SCAP in parental HeLa (control) and shSCAP HeLa cells, as measured by Western blotting. Data are mean ± s.e.m. (n = 4 independent experiments, ***$P < 0.001$, two-tailed Student's *t*-test). Asterisks on the Western blot denote nonspecific bands. **e**, Total cholesterol levels in parental HeLa and shSCAP HeLa cells. Data are means ± s.e.m. (n = 3 independent experiments, NS, not significant, two-tailed Student's *t*-test). **f**,**g**, PI4P staining in parental HeLa and shSCAP HeLa cells with (**g**) or without (**f**) sialyltransferase (ST)-mRFP expression. N, nucleus. Scale bars, 10 μm. **h**, BiFC visualization of OSBP/VAP-A interactions in control and SCAP knockdown cells. HeLa cells stably coexpressing Vn-OSBP and Vc-VAP-A were transfected with siRNA. After 72 h, the cells were treated with or without 2 μg/mL 25-HC for 2.5 h. High

magnifications of the boxed areas are shown in the insets where brightness/contrast-enhancement was applied. The graph shows the percentage of cells with the peripheral BiFC signal of Vn-OSBP/Vc-VAP-A. Data are means ± s.e.m. (n = 3 independent experiments, 100-131 cells per condition, ***$P < 0.005$, two-tailed Student's *t*-test). **i**, Close apposition of CD63- but not of TGN46-positive membranes to the peripheral BiFC signal of Vn-OSBP/Vc-VAP-A in SCAP knockdown cells treated with 2 μg/mL 25-HC for 2.5 h. Scale bars, 10 μm (large panels), 5 μm (insets).

Fig. 4 | SCAP is required for the biogenesis of CARTS at the TGN. a, Close proximity of CARTS formation sites to VAP-A/OSBP-mediated ER-Golgi contact sites. HeLa cells stably coexpressing Vn-OSBP and Vc-VAP-A were transfected with a plasmid for PAUF-MycHis. After 20 h, the cells were treated with 2 μg/mL 25-HC for 2.5 h. Images were subjected to deconvolution processing as described in *Online Methods*. N, nucleus. High magnifications of the boxed areas are shown in the bottom row. Arrowheads indicate putative nascent CARTS located in the close vicinity of the BiFC signal of Vn-OSBP/Vc-VAP-A. Scale bars, 5 μm (upper row), 2.5 μm (bottom row). **b**, PAUF-MycHis secretion in control (Cont) and SCAP knockdown cells, monitored by Western blotting. The graph shows quantification of secreted PAUF-MycHis relative to the total cellular level and normalized as the values in control cells. Data are means ± s.e.m. (n = 3 independent experiments, **$P < 0.01$, two-tailed Student's *t*-test). **c**, Biogenesis of mKate2-FM4-PAUF-containing CARTS in control and SCAP knockdown cells. The cells were incubated at 20°C with the D/D solubilizer and cycloheximide (CHX) for 45 min, followed by incubation at 37°C for 5 or 15 min. The graph shows the number of mKate2-FM4-PAUF-containing CARTS in control and SCAP knockdown cells at 15 min after the temperature shift to 37°C. Data are means ± s.e.m. (control siRNA: n = 20 cells; SCAP siRNA: n = 29 cells, ****$P < 0.0001$, two-tailed Student's *t*-test). Scale bar, 10 μm. **d**, mKate2-FM4-GPI transport from the ER to the PM via the Golgi complex in control, SCAP, and VAP-A/B knockdown cells. The cells were incubated at 37°C with the D/D solubilizer and cycloheximide, and fixed at the indicated times. The graph shows the percentages of cells with mKate2-FM4-GPI

at the ER, ER/Golgi, Golgi/ PM, or PM at the indicated times. The data shown are for a single representative experiment out of three performed (control siRNA: 30 min, n = 235 cells; 60 min, n = 239 cells; 90 min, n = 252 cells; SCAP siRNA: 30 min, n = 248 cells; 60 min, n = 246 cells; 90 min, n = 241 cells; VAP-A/B siRNA: 30 min, n = 230 cells; 60 min, n = 238 cells; 90 min, n = 240 cells). Scale bar, 10 μm. **e**, mKate2-FM4-GPI has accumulated at the TGN at 90 min after the transport induction in SCAP knockdown cells. N, nucleus. Scale bar, 10 μm.

Fig. 5 | SCAP regulates CARTS biogenesis in a cholesterol-dependent manner. a, Schematic representation of the SCAP topology, where the Y234 and Y298 residues, loop1 and loop7, and WD (tryptophan–aspartate) repeats are indicated. **b**, Establishment of shSCAP HeLa cells stably expressing the hamster SCAP WT, Y234A or Y298C mutant. Cell lysates were immunoblotted (IB) with the indicated antibodies. Ham, hamster; Hum, human. **c**, Recovery of PI4P turnover on expression of hamster SCAP WT, but not of Y234A or Y298C. **d**, Recovery of biogenesis of mKate2-FM4-PAUF-containing CARTS on expression of hamster SCAP WT, but not of Y234A or Y298C. The graph shows the number of mKate2-FM4-PAUF-containing CARTS in the indicated cells at 15 min after the temperature shift to 37°C. Data are means ± s.e.m. (n = 20 cells per conditions, ****$P < 0.0001$, two-tailed Student's *t*-test). Scale bars, 10 μm.

Fig. 6 | Working model for the facilitation of CARTS biogenesis by SCAP at ER-Golgi contact sites. When the ER cholesterol (Chol) level is low, SCAP escorts SREBP transcription factors from the ER to the Golgi complex for cholesterol synthesis and uptake (left panel, blue arrows). When the ER contains a sufficient level of cholesterol, cholesterol-bound SCAP interacts with the VAP/OSBP complex via Sac1, and functions in the counter transport of ER cholesterol and Golgi PI4P at ER-Golgi contact sites to promote CARTS biogenesis at the TGN domains immediately adjacent to the ER contacts sites (left panel, red arrow, and right panel). Ceramide (Cer) transported by the VAP/CERT complex is metabolized together with phosphatidylcholine (PC) to

SM and DAG. Cholesterol and SM organize lipid nanodomains for processing and sorting of cargoes. DAG recruits PKD for membrane fission.

Supplementary Fig. 1 | Sac1 does not interact with the OSBP PH-FFAT mutant. **a**, Interactions of FLAG-Sac1 with VAP-A and Myc-OSBP WT, but not with the PH-FFAT mutant in HEK 293T cells. Cell lysates were subjected to immunoprecipitation with an anti-FLAG M2 affinity gel, and the cell lysates (Input) and immunoprecipitates (IP) were immunoblotted (IB) with the indicated antibodies. The interaction with VAP-A was enhanced by coexpression of FLAG-Sac1 with Myc-OSBP WT, but not with PH-FFAT. Single and double asterisks denote degraded Myc-OSBP fragments and the immunoglobulin heavy chain, respectively. **b**, A schematic representation of the SCAP interactions with VAP, OSBP, and Sac1.

Supplementary Fig. 2 | BiFC visualization of VAP-A, OSBP, and Sac1 interactions at ER-Golgi contact sites. **a**,**b**, No BiFC signal in HeLa cells with single expression of Venus N-terminal fragment (Vn)-fused proteins (**a**) or Venus C-terminal fragment (Vc)-fused proteins (**b**). **c**,**d**, BiFC visualization of OSBP/VAP-A (**c**) and OSBP/Sac1 (**d**) interactions at ER-Golgi contact sites. The coexpression of Vn-OSBP (WT or FF/AA) with Vc-VAP-A (**c**) or Vc-Sac1 (**d**) was visualized with an anti-GFP antibody. The BiFC signal was enhanced by treatment of cells with 2 μg/mL 25-HC for 2.5 h. Vn-OSBP FF/AA showed a reduced BiFC signal, compared with the WT. Scale bars, 10 μm.

Supplementary Fig. 3 | Sterol-dependent localization of SCAP. **a**,**b**, Localization of stably expressed GFP-SCAP in HeLa cells with or without cholesterol depletion (Chol Depl) for 3 h or treated with 2 μg/mL 25-HC for 2.5 h. Accumulation of GFP-SCAP in GM130 (*cis*-Golgi matrix protein)- and Mannosidase II (*cis*/*medial*-Golgi marker enzyme)-positive membranes upon cholesterol depletion for 3 h (**b**). N, nucleus. **c**, Proteolytic activation of SREBP2 upon cholesterol depletion (Chol Depl), monitored by Western blotting with an anti-SREBP2 antibody. Arrowheads indicate the precursor

(P) and mature (M) forms of SREBP2. Asterisks denote nonspecific bands. Scale bars, 10 μm.

Supplementary Fig. 4 | Knockdown of ER-Golgi contact site components impairs PI4P turnover. PI4P staining in control (Cont), VAP-A/B, CERT/OSBP, and Sac1 knockdown cells. Scale bar, 10 μm.

Supplementary Fig. 5 | Establishment of a HeLa stable cell line coexpressing Vn-OSBP and Vc-VAP-A. The cells were treated with or without 2 μg/mL 25-HC for 2.5 h. Scale bar, 10 μm.

Supplementary Fig. 6 | Lipid transfer at ER-Golgi contact sites is required for GPI-anchored protein transport from the TGN to the PM. a, mKate2-FM4-GPI transport from the ER to the PM via the Golgi complex in control (Cont), OSBP, and CERT/OSBP knockdown cells. The cells were incubated at 37°C with the D/D solubilizer and cycloheximide, and fixed at the indicated times. The graph shows the percentages of cells with mKate2-FM4-GPI at the ER, ER/ Golgi, Golgi/PM, or PM at the indicated times. The data shown are for a single representative experiment out of three performed (Cont siRNA: 30 min, n = 240 cells; 60 min, n = 230 cells; 90 min, n = 233 cells; OSBP siRNA: 30 min, n = 254 cells; 60 min, n = 229 cells; 90 min, n = 238 cells; CERT/OSBP siRNA: 30 min, n = 268 cells; 60 min, n = 235 cells; 90 min, n = 245 cells). **b**, mKate2-FM4-GPI transport in the presence or absence of the Myc-OSBP PH-FFAT mutant. Asterisks denote cells coexpressing mKate2-FM4-GPI and Myc-OSBP PH-FFAT. Scale bars, 10 μm.

Supplementary Fig. 7 | CARTS transport GPI-anchored proteins. a, Colocalization of PAUF-MycHis and mKate2-FM4-GPI in CARTS at 30 min after transport induction. **b**, Colocalization of GST-PKD2-kinase dead (KD) and mKate2-FM4-GPI in tubules attached to the TGN at 90 min after transport induction. In **a** and **b**, high magnifications of the boxed areas are shown in the right column where brightness/contrast-

enhancement is applied to the mKate2-FM4-GPI channel. Arrowheads indicate a GST-PKD2-KD-induced tubule containing mKate2-FM4-GPI. Scale bars, 10 μm

Supplementary Fig. 8 | Localization of the stably expressed hamster SCAP WT, Y234A, and Y298C mutants in shSCAP HeLa cells. The cells were subjected or not to cholesterol depletion (Chol Depl) for 3 h. Merged images for the hamster SCAP WT, Y234A or Y298C (green) and the *cis*/*medial*-Golgi marker GPP130 (magenta) of the boxed areas are shown in the insets. Scale bars, 10 μm.

Supplementary Video 1 | The biogenesis of mKate2-FM4-PAUF-containing CARTS at the TGN. HeLa cells expressing mKate2-FM4-PAUF were first incubated at 20°C for 45 min. Images were acquired continuously after the temperature shift to 37°C with a time interval between frames of 30 sec for ~75 min. N, nucleus.

Fig. 1

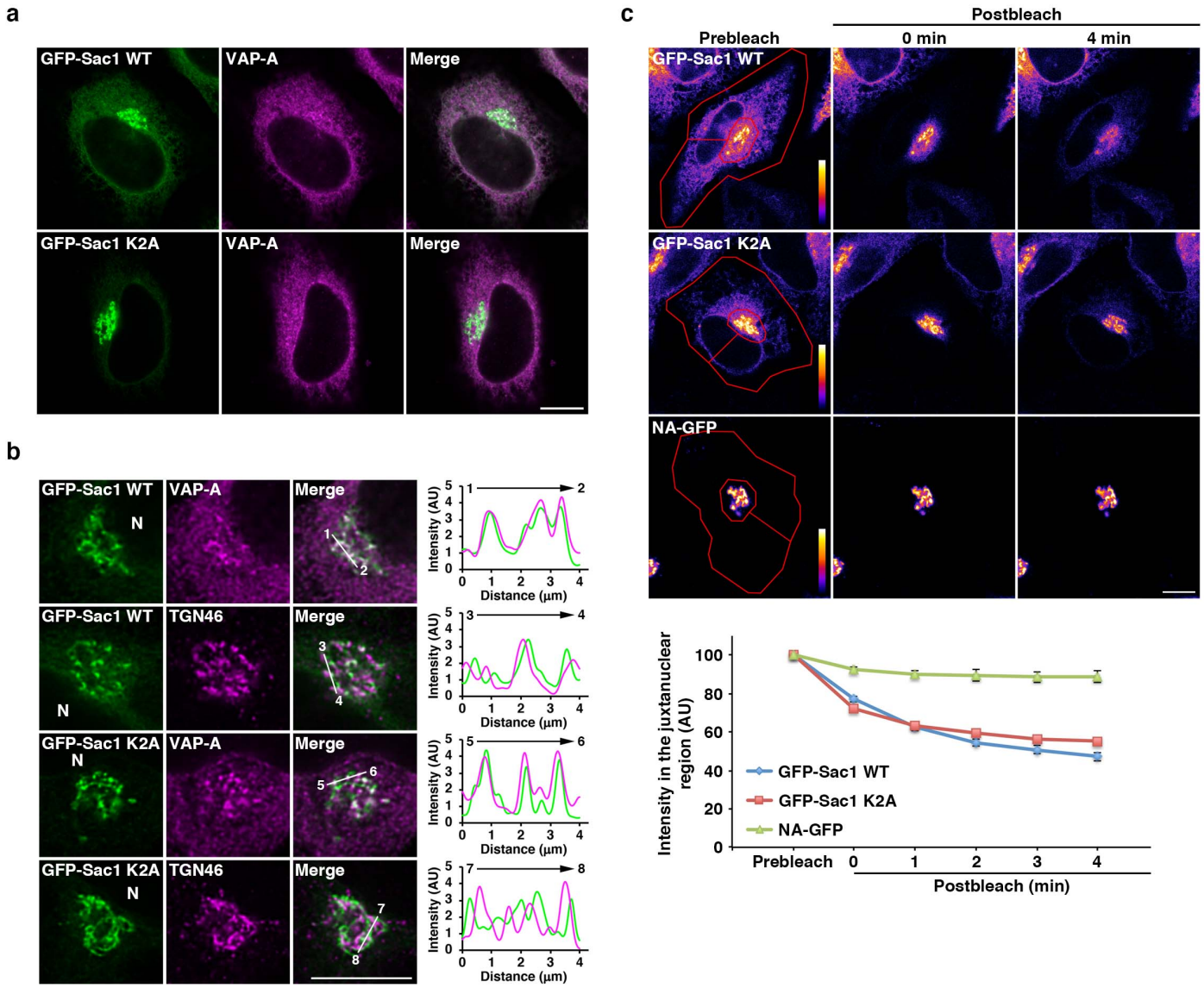

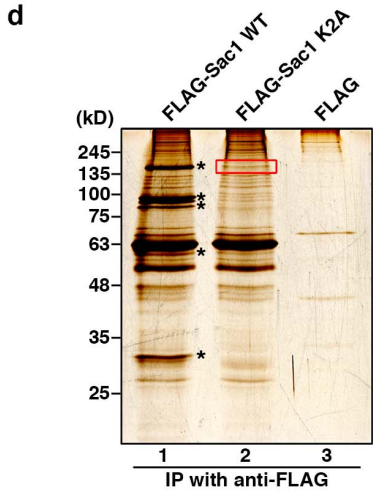

e

VAP-A
27-38: GPFTDVVTTNLK
115-125: EAKPDELMDSK
139-146: LNDMEPSK
147-154: AVPLNASK

VAP-B
20-31: GPFTDVVTTNLK
140-147: IISTTASK
148-155: TETPIVSK
201-216: TVQSNSPISALAPTGK

OSBP
205-212: TELQNTLR
218-230: VEDLSTCNDLIAK
238-246: SLSELESLK
247-254: LPAESNEK
304-313: LEETLEQLAK
324-340: GATVLPANTPGNVGSGK
377-395: TGSNISGASSDISLDEQYK
626-637: KVTGEVTDPSGK
627-637: VTGEVTDPSGK
729-736: WDEANAEK
757-768: ATEDGTPYDPYK

SCAP
47-62: LPLPGTGPVEFTTPVK
63-73: DYSPPPVDSDR
108-116: NLLAVDVFR
122-130: AFQLVEEIR
202-210: TLQTSATLK
211-219: DLLFGVPGK
367-378: SVVSTPVDLEVK
887-896: SSQPTQPEPR
1092-1102: LVTGSQDHTLR

Fig. 2

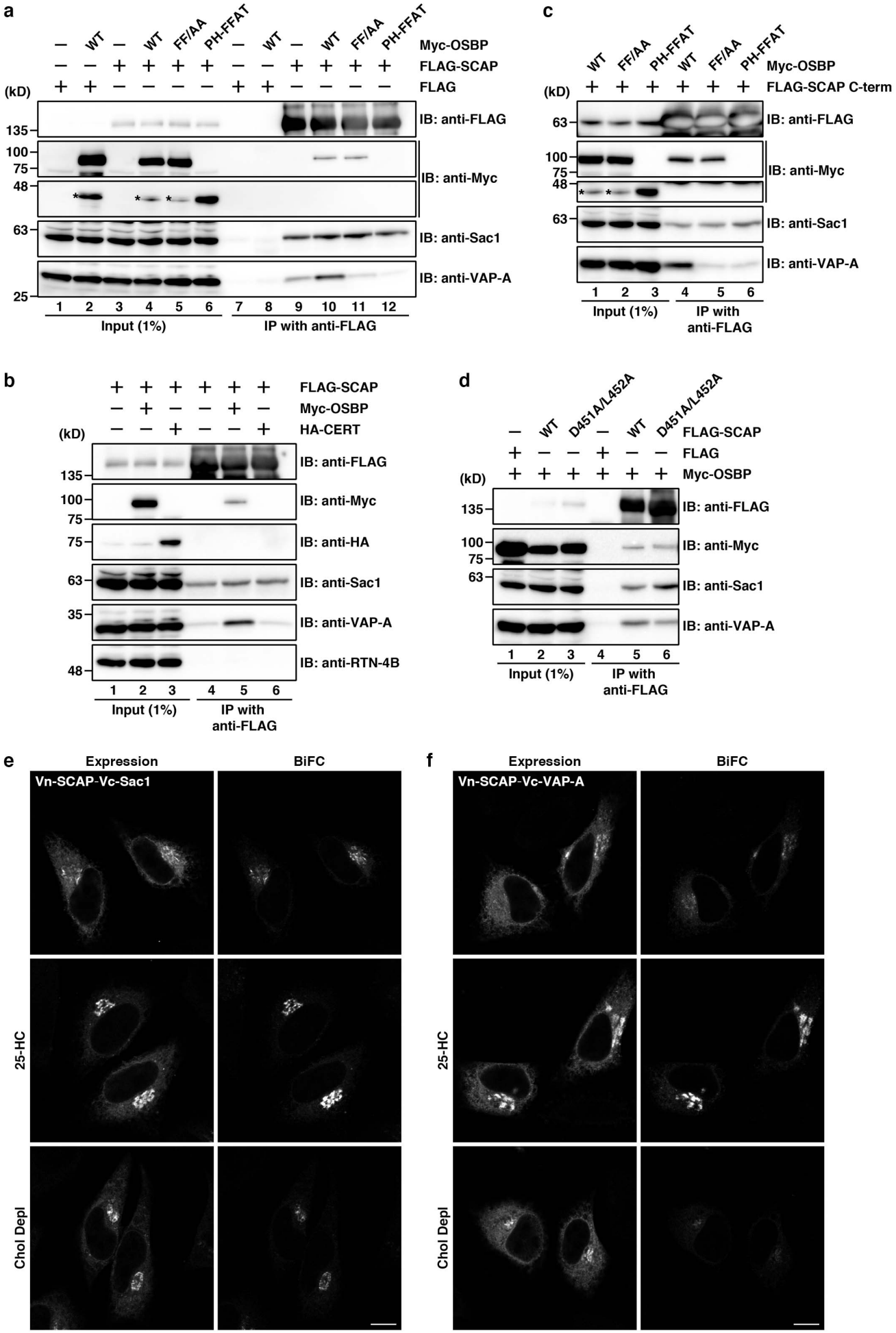

Fig. 3

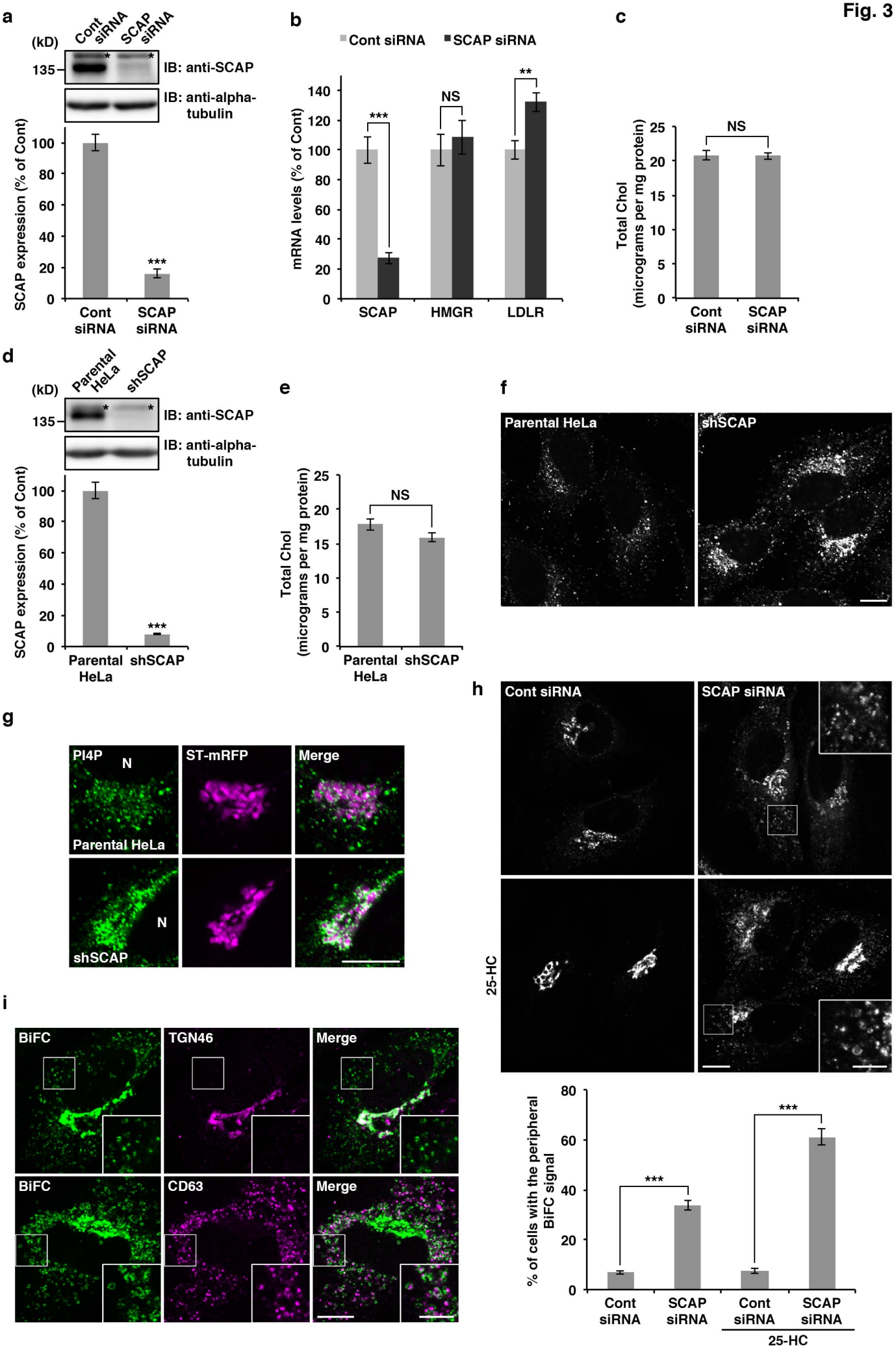

Fig. 4

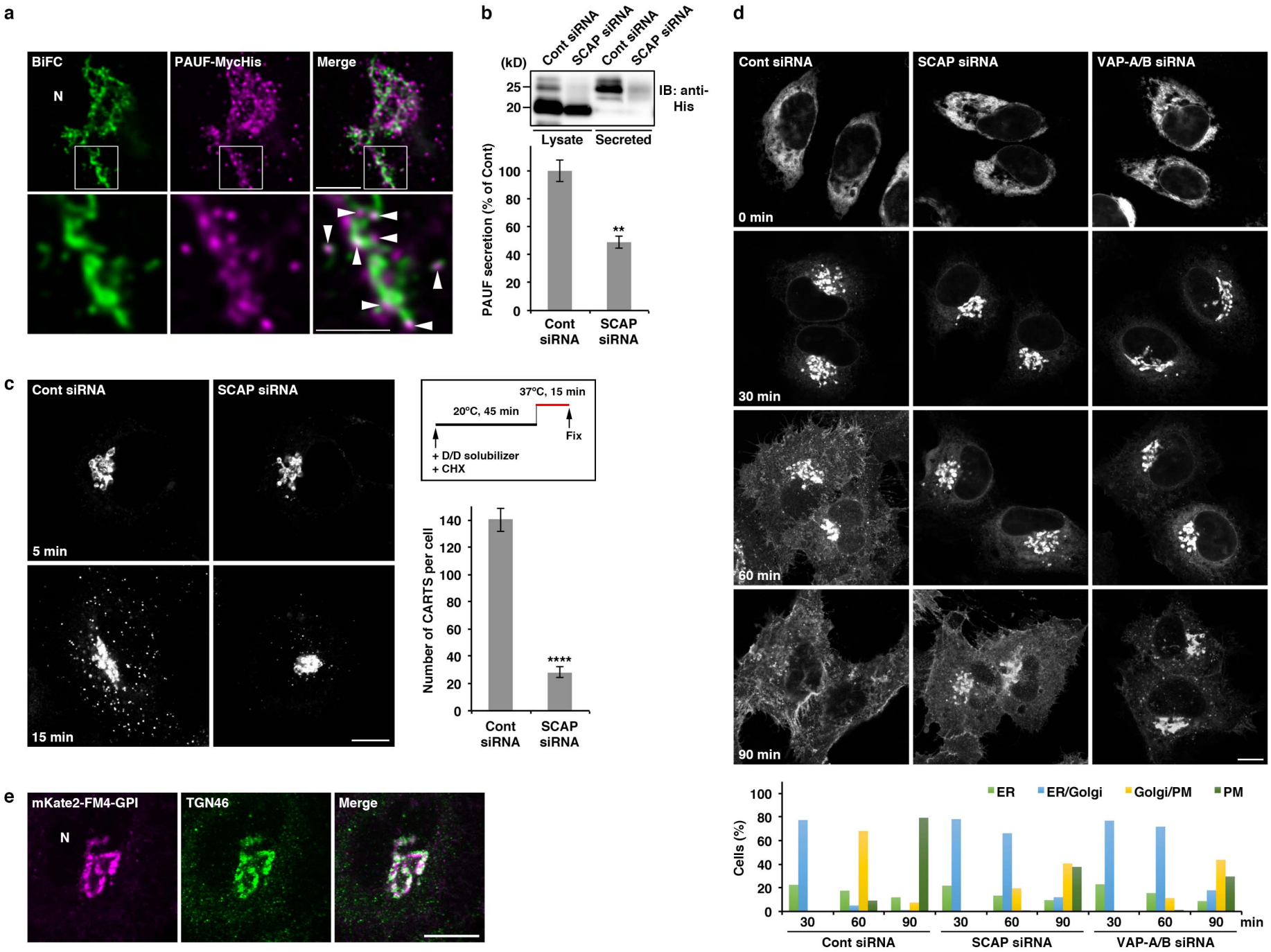

Fig. 5

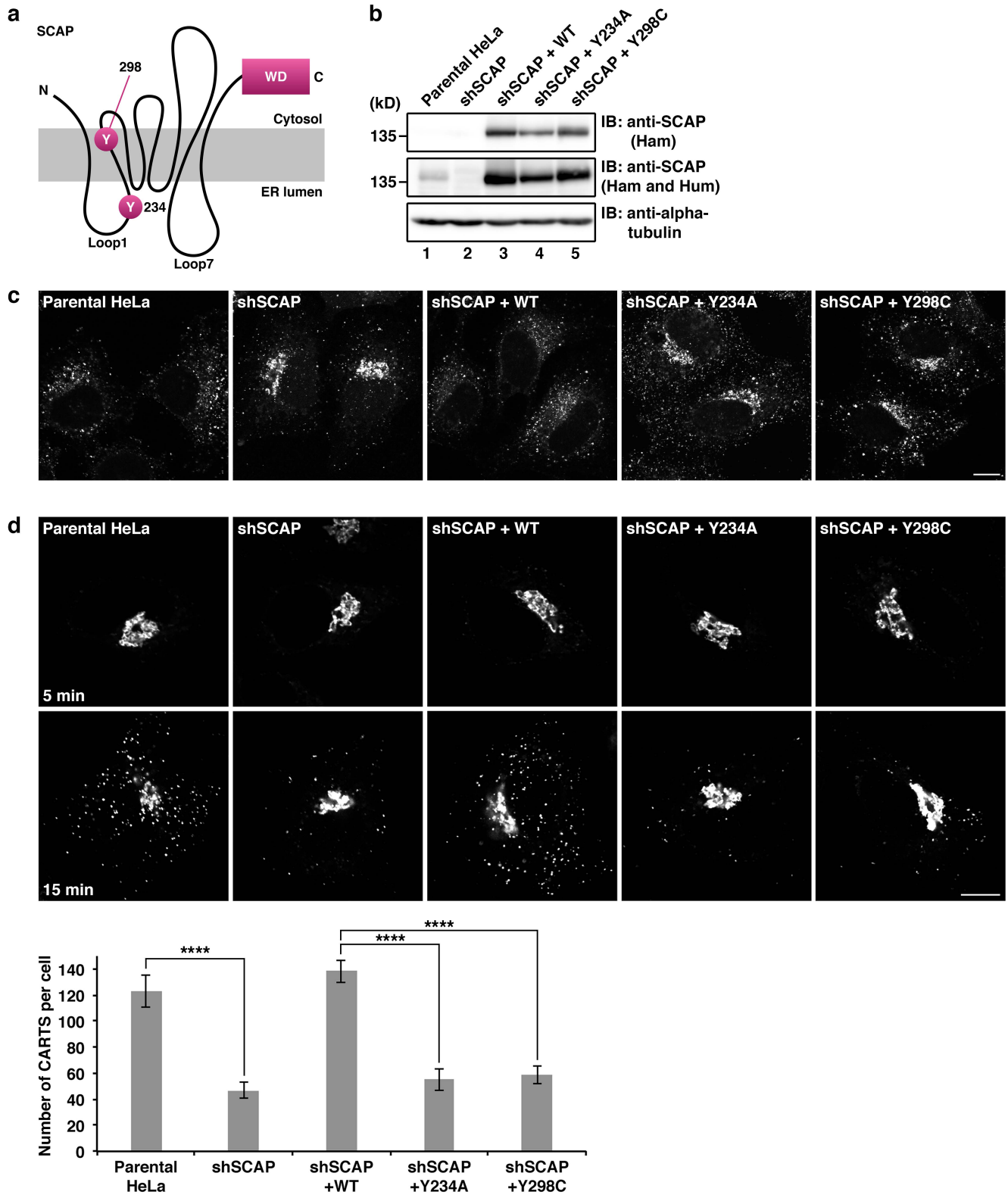

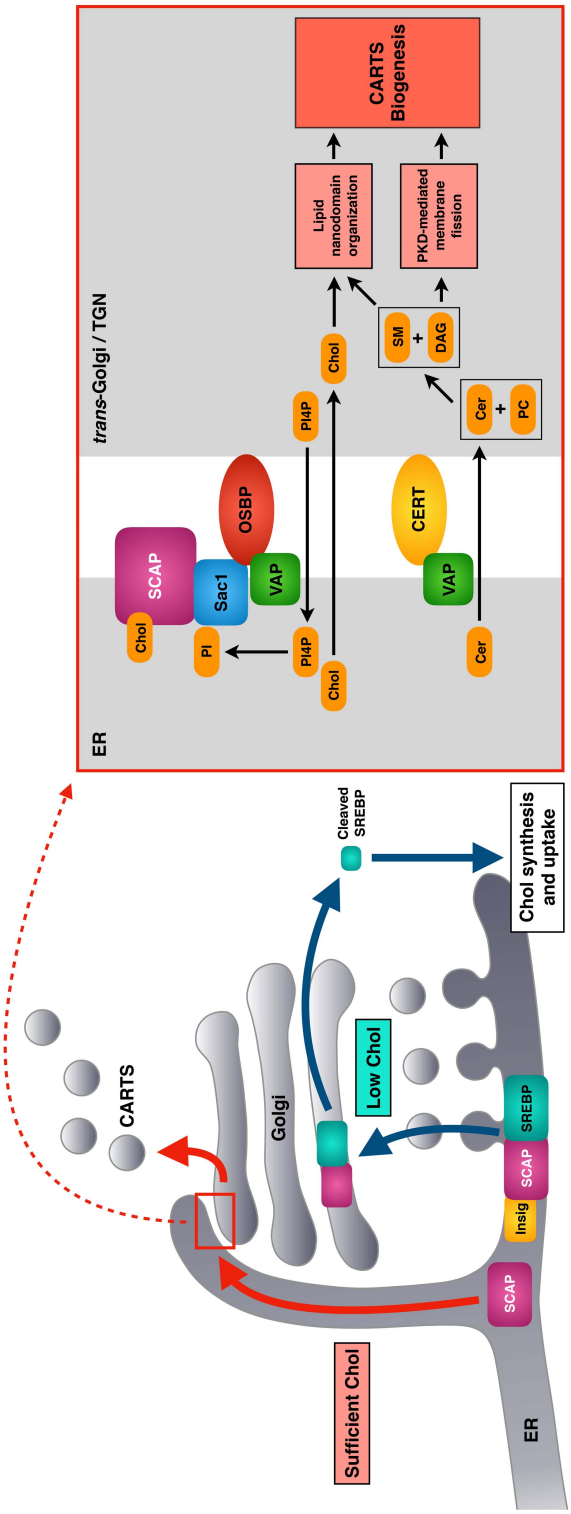

Fig. 6

Supplementary Fig. 1

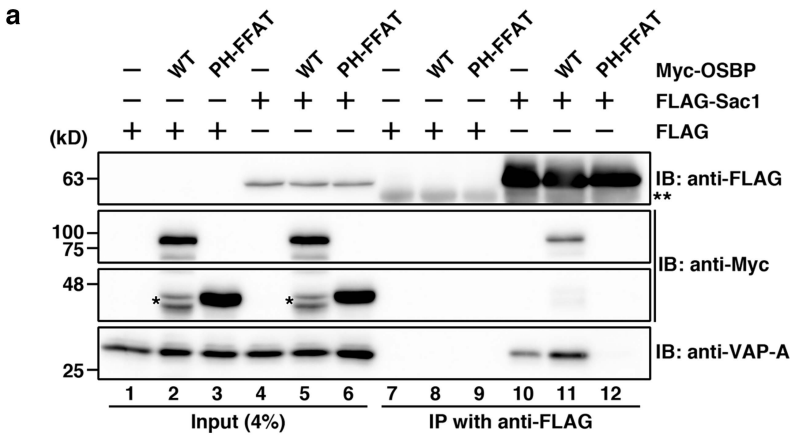

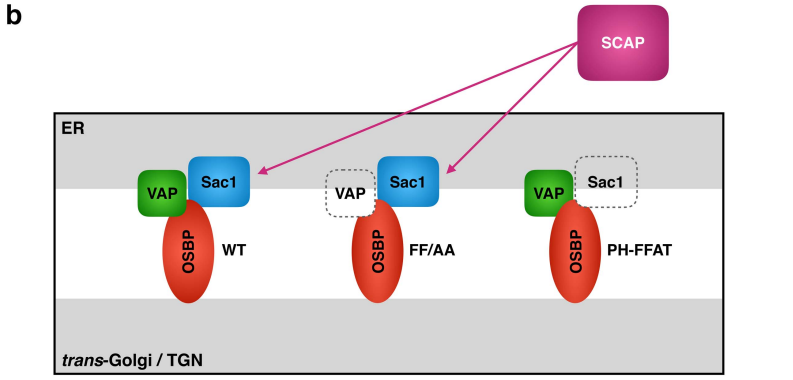

Supplementary Fig. 2

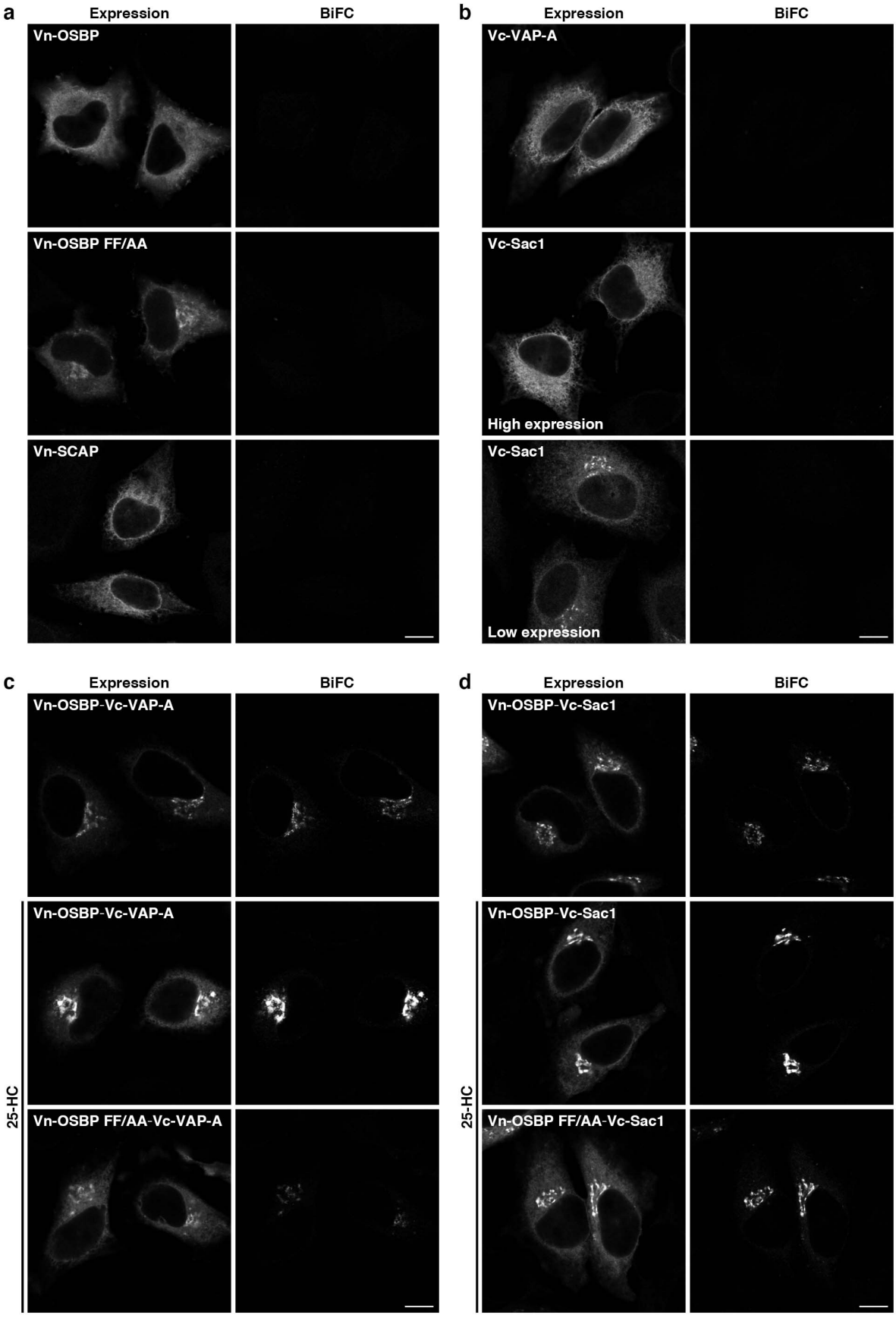

Supplementary Fig. 3

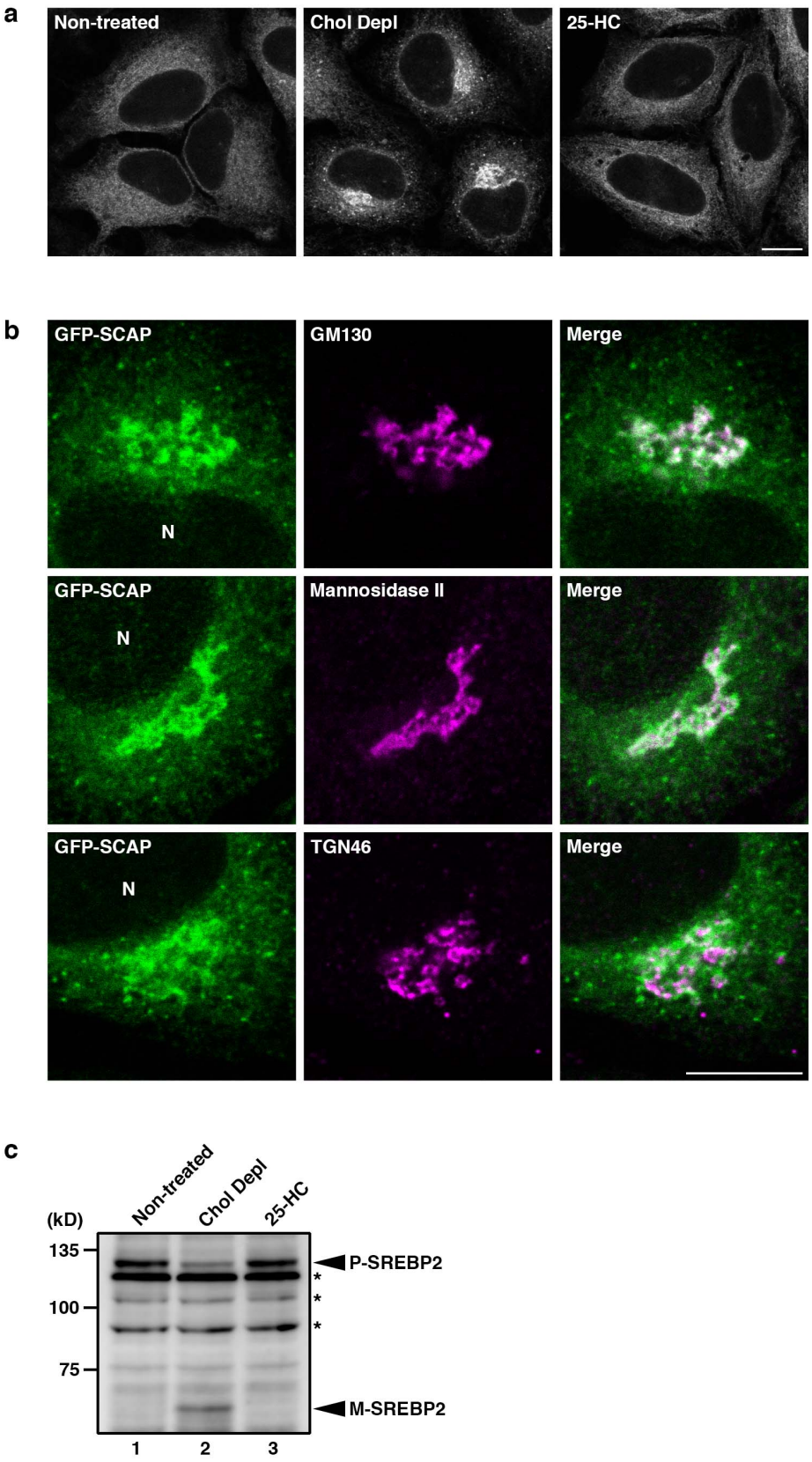

Supplementary Fig. 4

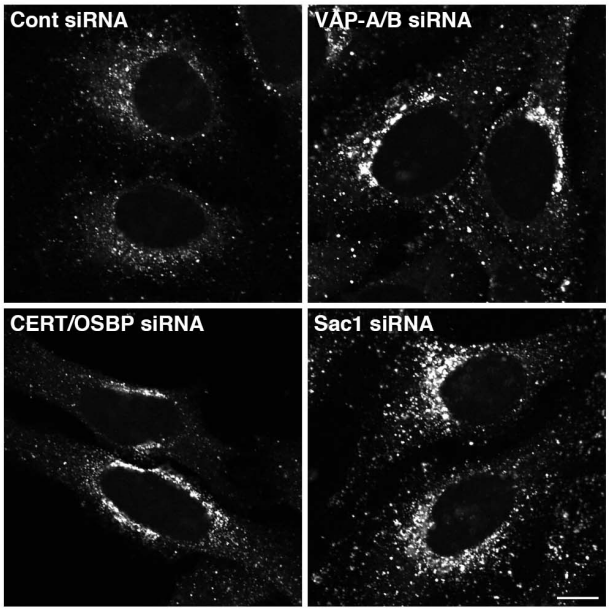

Supplementary Fig. 5

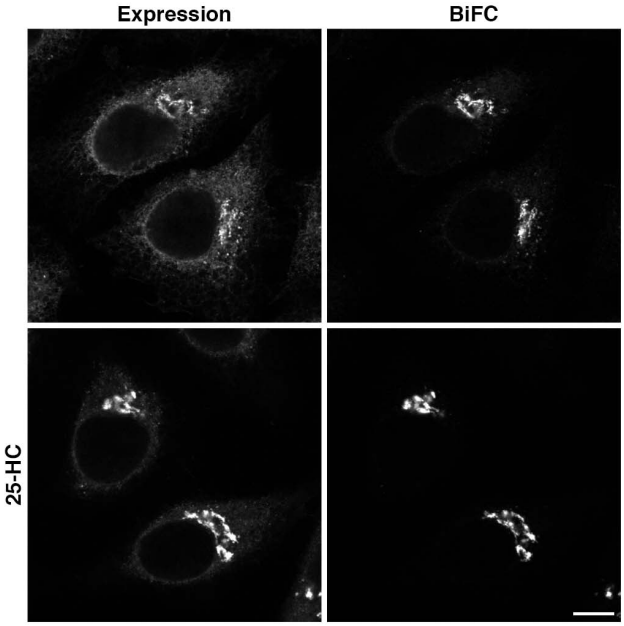

Supplementary Fig. 6

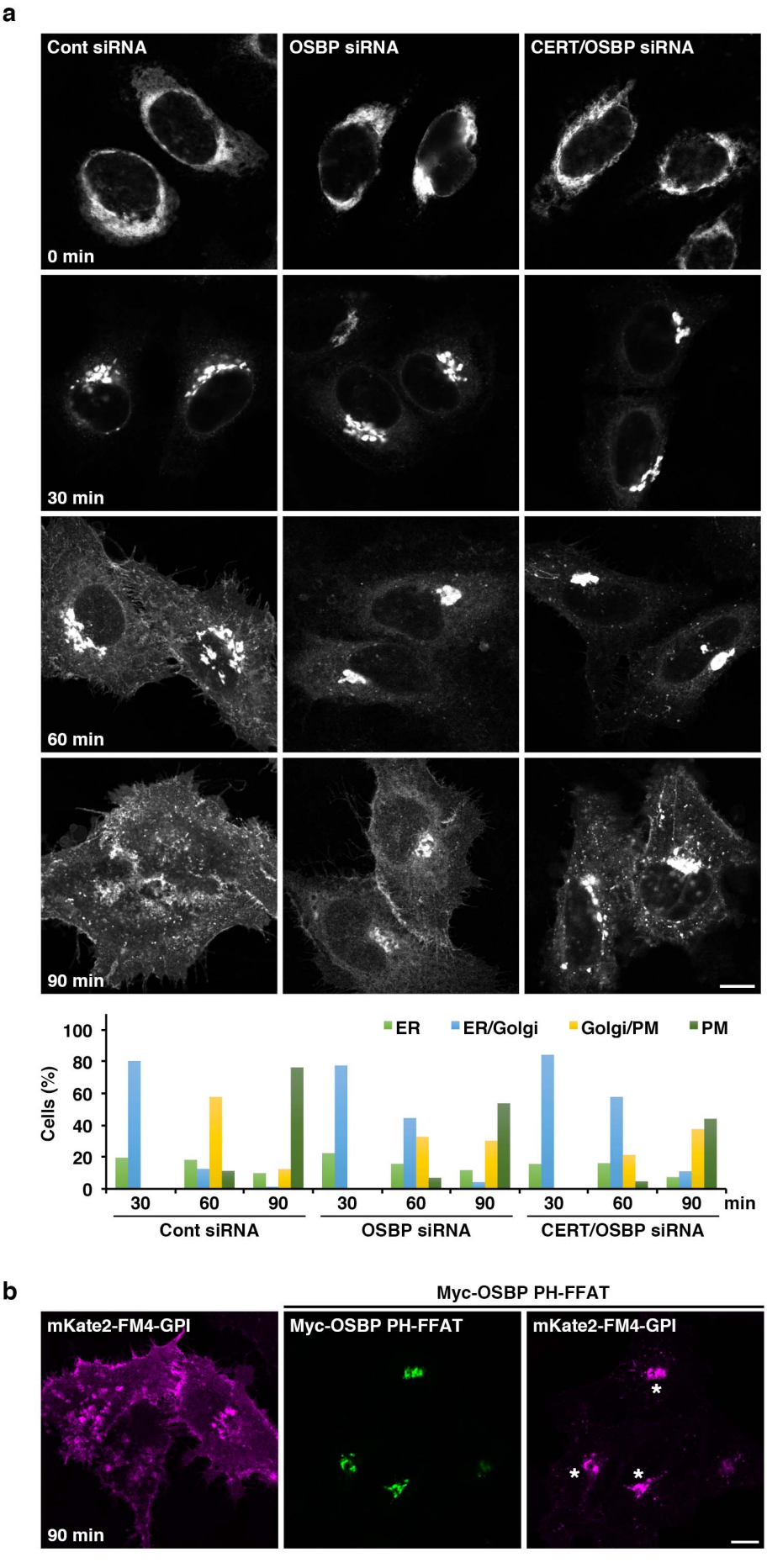

Supplementary Fig. 7

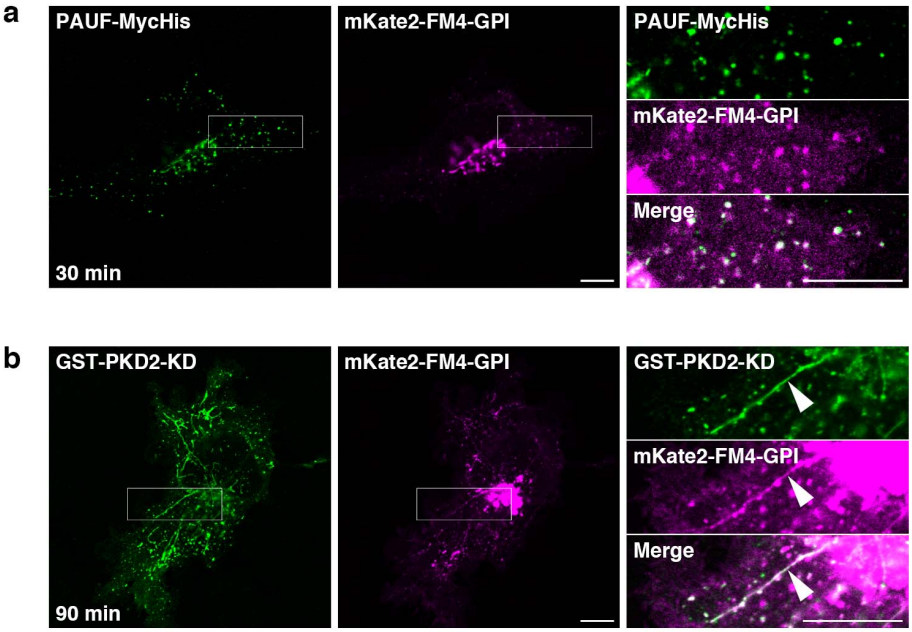

Supplementary Fig. 8